HYPERFINE INTERACTION STUDIES OF IRON COMPOUNDS BY MÖSSBAUER EFFECT

Thesis submitted to the
University of Roorkee
for the award of the
Degree of Doctor of Philosophy
in
Physics

KAILASH CHANDRA

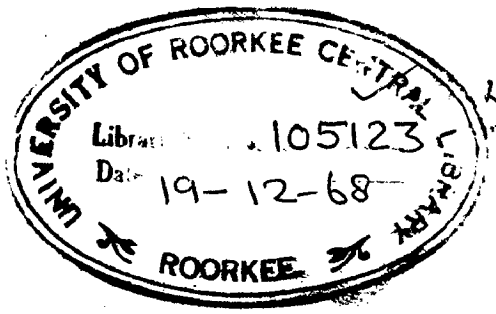

DEPARTMENT OF PHYSICS
UNIVERSITY OF ROORKEE
ROORKEE (INDIA)
1967

C E R T I F I C A T E

Certified that the thesis entitled " Hyperfine Interaction Studies of Iron Compounds by Mössbauer Effect" which is being submitted by Sri Kailash Chandra in fulfilment for the award of the Degree of Doctor of Philosophy in Physics of University of Roorkee, Roorkee is a record of his own work carried-out by him under my supervision and guidance. The matter embodied in this thesis has not been submitted for the award of any other Degree.

This is further to certify that he has worked for a period equivalent to 24 months full time research for preparing his thesis for Ph.D. Degree at the University.

S. P. Puri

(S.P.Puri)
Department of Physics
University of Roorkee
Roorkee (India)

Dated Sept. 11, 1967

ACKNOWLEDGEMENTS

I feel it incumbent upon me to convey my deep sense of gratitude to Dr. S.P. Puri, for suggesting the problems and continuous supervision and guidance throughout the course of this work. Without his stimulating discussions and continuous inspiration the work reported herein would not have been possible.

My sincere thanks are due to Dr. V.K.S. Dave of Geology Department for his kind help in determining the crystal axes. The author is specially grateful to his coworkers Deo Raj and V.K. Garg for their continuous cooperation in the experimental work and discussions. Furthermore I thank S.N. Singh and S.P. Taneja for helpful discussions and assistance at the time of writing this thesis.

I express my indebtedness to the Head of the Physics Department for his interest and encouragement in the progress of this work and for providing the laboratory facilities.

Last but not the least, I acknowledge the financial help from the Council of Scientific and Industrial Research, New Delhi, in awarding me the junior and senior research fellowships successively.

Kailash Chandra

(Kailash Chandra)

TABLE OF CONTENTS

C H A P T E R I

PRELIMINARIES AND STATEMENT OF THE PROBLEM

1. THE MÖSSBAUER EFFECT

(i) General Discussion

The phenomenon of resonance fluorescence in atomic systems[1] and nuclear systems[2] has been known for many years. Previous to Mössbauer's discovery[3] the following methods were employed to compensate for the nuclear recoil so as to achieve resonance absorption of γ-rays:

(a) Centrifuge[2]. The emitter or the target was mounted on a centrifuge which is mechanically rotated with such a speed as to compensate for the nuclear recoil. The required speeds are of the order of 10^5 cm/sec.

(b) Heat[4]. Thermal motion is used to compensate for the recoil.

(c) Previous Recoil[5]. The recoil due to previous emission of a γ-quantum or β is used to compensate for the recoil in the subsequent γ-emission.

While studying the scattering of 129 keV gamma rays of Ir^{191} by Ir and Pt, R.L. Mössbauer found an unexpected increase in scattering in Ir at low temperatures. Subsequently the discoverer himself advanced an interpretation of his observation, based on Lamb's article[6] "Capture of Neutrons by Atoms in a Crystal". He found that if a solid source cooled to sufficiently low temperatures was used

the recoil is completely eliminated. The reason is simple to understand. Under suitable conditions, the crystal binding is effective and so not only the emitting nucleus, but the crystal as a whole takes part in recoil. Even for a microcrystal the recoil is negligibly small. However for efficient resonance absorption, one still has to compensate for the natural line width, Γ .

This discovery made available the purest radiation and stimulated interest in hitherto desirable but unattempted fields like the phonon spectrum of a solid, the anisotropy of binding forces of atoms in solids, Gravitational red shift and hyperfine interactions etc., so much so that Mössbauer became a co-sharer of Nobel Prize for Physics in 1961.

Since the discovery of Mössbauer effect a large number of review articles[7-11] and proceedings of a series of international conferences[12-17] held on Mössbauer effect have appeared in the short span of 7 years.

When a free nucleus emits γ-rays of energy, E, it recoils with kinetic energy R($= \frac{E}{2\ mc^2}$). Thus a free nucleus having states of internal energy E_1 and E_2, the emitted photon energy is not E_2-E_1, but less by R, the energy which is perforce transmitted to the emitting nucleus as a consequence of energy and momentum conservation between the nucleus and emitted photon. If however the nucleus is bound in a crystal there can be substantial probability for emission of a photon without this recoil

energy shift. Same is true in the case of absorption of this energy by a similar nucleus. The energy and momentum conservation in Mössbauer effect have been discussed both by Weisskoff[18] and Lipkin[19] in a strikingly interesting manner. Quantum mechanically we can understand the phenomenon as follows: For an atom bound in a solid the wave function is confined to a region of space of size Δx, and is consequently not a momentum eignfunction, but has an uncertainty of momentum $\frac{\hbar}{\Delta x}$. If this uncertainty is larger than the momentum $\hbar k$ for the γ-rays, there will be a good chance of absorbing the recoil without changing the state of the atom. The condition for a large fraction of recoilless emission is thus $k \Delta x \leq 1$. Quantitatively, if the initial wavefunction of the atom is ψ_i , the wavefunction just after emission is, in the impulse approximation, $e^{ik.r}\psi_i$, so that the chance of finding that atom in the same state after emission is

$$\left| \int \psi_i^* e^{ik.r} \psi_i \, d^3\bar{r} \right|^2$$

If the initial states are occupied with Gaussian probability distribution p_i with mean square displacement $\langle x^2 \rangle$ in the direction of $\bar{k}$, the fraction of recoilless γ-ray is

$$f = \exp\left[-k^2 \langle x^2 \rangle\right] \qquad (1)$$

We may point out that the term "recoilless emission" is misleading. The lattice as a whole (the lattice centre of mass) always recoil after phonon emission, whether or not there is Mössbauer effect. The Mössbauer effect, rather,

is photon emission without transfer of energy to internal degrees of freedom of the lattice (zero phonon process). In order to explain how recoilless processes are possible we must understand the way by which energy may be transmitted from a nucleus to the lattice in which it is bound. It is often desirable to use Debye approximation to understand the phenomenon and to express Eq.1 to more familier quantities. According to Debye model, the fraction of decays which take place without recoil depends on the ratio of free atom recoil energy E_γ, to the Debye energy $k\theta_D$, the quantum of vibrational energy of the lattice structure. An atom in the solid may be thought of as being free to emit zero, one, or many phonons, but as being unable to recoil with an arbitrary energy. The recoilless fraction f is unity for a perfect lattice. In a general lattice $f < 1$ and in Debye approximation it is given by[11] (for $\theta_D > T$)

$$f = e^{-2W}$$

where

$$2W = \frac{E_\gamma}{k\theta_D}\left\{\frac{3}{2} + \frac{\pi^2 T^2}{\theta_D^2}\right\} \qquad (2)$$

This is the familiar form for the Debye Waller factor 2W. The characteristic values for f are 0.91 for 14.4 keV γ-ray of Fe^{57} and 0.06 for the 129 keV γ-ray of Ir^{191} both for the natural metallic host lattice. In actual experiments the Debye Waller factors of the source and the absorber jointly determine the magnitude of the observable effect.

The observation of Mössbauer effect is accomplished by measuring the change in transmission (or scattering) of gamma rays emitted without recoil as a function of the velocity with which the source and absorber (or scatterer) move relative to each other. The relative motion between the source and absorber produces a Doppler shift $\frac{v}{c} E_\gamma$ of the energy of the emitted -ray with respect to the absorption level, and therefore a change in the rate of absorption or scattering. If the source (or absorber) emits (or absorbs) γ-rays of several different energies of the order $E_\gamma \pm \frac{v}{c} E_\gamma$, then such structure will appear as resonance lines in a plot of counting rate as a function of the Doppler velocity.

For the choice of nuclides to be used in Mossbauer experiments several considerations are required to be kept in view. The dependence of recoil free fraction f, upon the γ-ray energy practically excludes from consideration transition of over 150 keV; energies over 100 keV are practicall, only for the heavier nuclei ($A \simeq 150$). The transitions must end up in a stable configuration (ground state) and must decay through β^- emission, K capture, β^+ emission, or a metastable state from a parent having a sufficiently long half life in relation to its cost and ease of procurement. Life time of the (Mössbauer γ-ray) excited state which is related to the width of the state via the uncertainty principle, must lie within a few orders of magnitude of 10^{-8} sec. These are the major considerations

although few others e.g. maximum resonance cross-section σ_o , internal conversion coefficient α , the atomic scattering cross-section σ_{at} , and the relative abundance of the absorber state isotope are also of some importance when one comes to the details of actually observing the Mössbauer resonance.

Several tables have been published[7,10,11,20] listing nuclides possessing suitable values of the several parameters given above. Most have proved to give very small observed effects and of limited usefulness for solid state and nuclear studies. Several of these give small, but useful effects of estimating life times of excited states, Lamb-Mössbauer factors etc.. The most useful transitions have been those from low lying excited states in Fe^{57}, Sn^{119}, Dy^{161}, Tm^{169} and Au^{197} which have been used by investigators in both solid state and nuclear physics experiments. Of these, Fe^{57} has, by a considerable margin, received the most attention, with Sn^{119} a distant second in popularity. Fe^{57} Mössbauer isotope has the advantage of ease with which effect can be observed, the convenient linewidth, the relative long life time, and availability of the parent isotope (Co^{57}) and finally the fortuitous circumstances that iron is one of the transition metals (having an unfilled d-shell) which plays the principal role in a number of incompletely understood phenomena connected with magnetic ordering in solids.

Since we shall here be concerned only with Fe^{57}, it

will considerably facilitate our discussion henceforth to confine ourselves to a detailed exposition of the properties of this particular nuclide and the interaction with its environment. The radioactive parent of Fe^{57}, used in our experiments, is Co^{57}(270 days) which decays by electron capture into Fe^{57} according to the decay scheme shown in Fig.1. The 14.4 keV transition from the 3/2 excited state to ground state gives rise to the gamma ray used in Mössbauer experiments. The physical parameters which are of interest in these experiments are tabulated below:

Energy of γ-ray, E_γ	14.37 keV
Life time of excited state, $\tau_{1/2}$	1.0×10^{-7} sec
Natural line-width, Γ	4.6×10^{-9} eV $\simeq$ 0.1 mm/sec
Internal conversion coefficient, α	10
Spin and parity of ground state, I_g	$1/2^-$
Spin and parity of excited state, I_e	$3/2^-$
Maximum resonance cross-section, σ_o	1.5×10^{6} barns
Atomic scattering cross-section, σ_{at}	5.5×10^{3} barns
Nucleus recoil energy, E_R	2×10^{-3} eV
Natural abundance of stable Fe^{57}	2.2%
Inverse 'Q', $\frac{1}{Q} = \frac{\Gamma}{E}$	3×10^{-13}
Magnetic moment of ground state, μ_g	+0.0903 ± 0.0007 nm
Magnetic moment of excited state, μ_e	-0.1549 ± 0.0013 nm
Quadrupole moment (of excited state), Q	+0.40 barns[21]

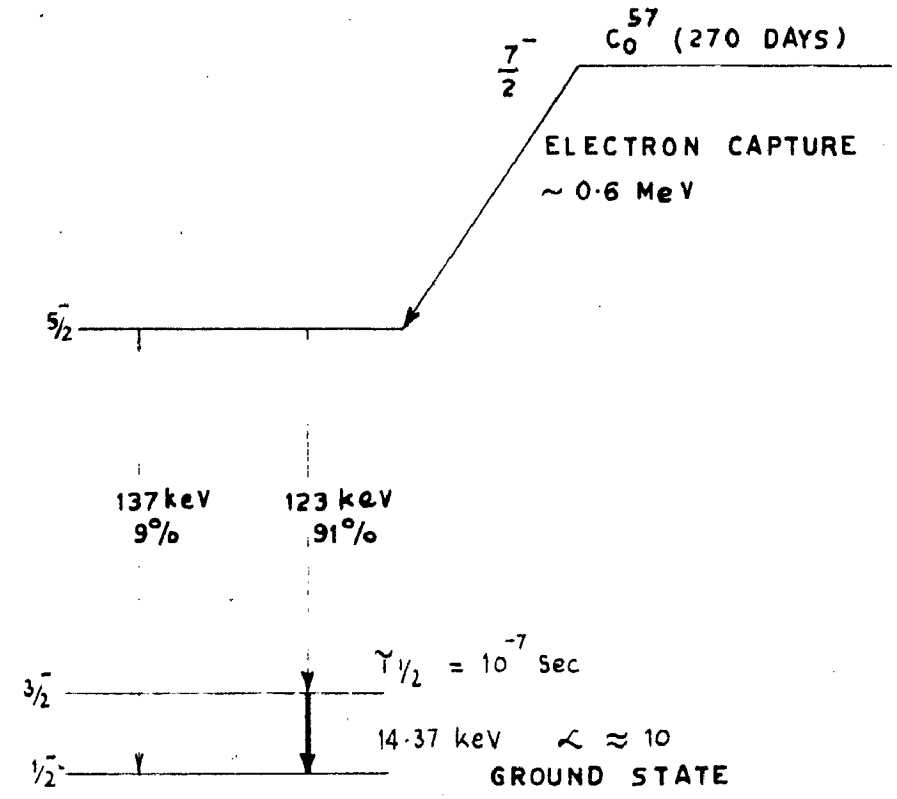

FIG. 1. DECAY SCHEME OF Co^{57} SHOWING THE 14·37 keV MÖSSBAUER TRANSITION.

(ii) Hyperfine Interactions

The property of zero-phonon γ-rays which has raised the importance of Mössbauer effect is to be found in the smallness of the linewidths. For most of the Mössbauer isotopes it is of the order of 10^{-8} eV or about 10^{-12} of the energy of the γ-ray. Electromagnetic radiations with comparable stability and linewidth have not yet been obtained by other means. Even the gas laser (optical maser) which is the best source of narrow-line infrared and visible radiation has not reached the resolution of stability of the Fe^{57} gamma ray energy. The salient feature is that the linewidth is small compared to the characteristic energies of interaction of nuclei with their surrounding electrons (hyperfine interactions). Therefore Mössbauer spectrometry makes it possible to determine the change in nuclear levels of the excited state and ground state, caused by the different chemical environments of the source and the absorber. These changes can occur as a result of three effects which can be described by considering the classical expression for the multipole moments of the charge distribution between the nucleus and the atomic electrons[22]

$$\phi = \sum_{n=0}^{\infty} \frac{e r^n}{d^{n+1}} P_n(\cos\theta) \qquad (3)$$

where the potential ϕ is measured at distance d from a coordinate system containing a unit charge e at a distance r from the origin, with θ , the angle between r and d.

P_n is the Legendre polynomial of order n.

n = 0 represents a monopole interaction which considers a point charge in an electrostatic field of spherical electron density, $-e|\psi(0)|^2$, near the nucleus. The difference between the electrostatic interaction of a hypothetical point nucleus and one of the actual radius R, both having the same energy is[11,23]:

$$\delta E = \frac{2\pi}{5} Ze^2 |\psi(0)|^2 R^2 \qquad (4)$$

where Z is the atomic number. Since nuclear radii are different for ground state and excited state, the change in energy upon emission of the γ-ray in the source is:

$$\delta E_{ex} - \delta E_{gd} = \frac{2\pi}{5} Ze^2 |\psi(0)|^2 (R_{ex}^2 - R_{gd}^2) \qquad (5)$$

where the symbols 'ex' and 'gd' stand for the excited state and ground state respectively. If the chemical structure has an influence on $|\psi(0)|^2$ there will be a change in energy level differences between the source and absorber to give the isomer shift, I.S.,

$$\begin{aligned} I.S. &= \delta E_a - \delta E_s \\ &= \frac{4\pi}{5} Ze^2 R^2 \left(\frac{\delta R}{R}\right) \left\{ |\psi(0)|^2_{abs.} - |\psi(0)|^2_{source} \right\} \end{aligned} \qquad (6)$$

Furthermore the term corresponding to n = 1 in Eq.3 represents electric dipole moment which does not exist for a nucleus. However there is interaction between

nuclear magnetic dipole moment, $\bar{\mu}$, with the magnetic field, $\bar{H}$, due to atom's own electrons. The Hamiltonian for interaction is[11]:

$$\mathcal{H}_m = -\bar{\mu}\cdot\bar{H} = -g\mu_n \bar{I}\cdot\bar{H} \qquad (7)$$

and the energy levels are

$$E_m = -\frac{\mu H m_I}{I} = -g\mu_n H m_I \qquad (8)$$

where m_I is the magnetic quantum number and takes the $(2I+1)$ values of the total nuclear angular momentum; μ_n is the nuclear magneton, and g is the nuclear gyromagnetic ratio.

The term corresponding to n = 2 in Eq.3 represents the electric quadrupole moment. The interaction between the nuclear quadrupole moment, Q, and the gradient of the electric field due to atomic electrons is expressed by the Hamiltonian[11]:

$$\mathcal{H}_Q = \frac{e^2qQ}{4I(2I-1)}\left[3I_z^2 - I(I+1) + \frac{\eta}{2}(I_+^2 + I_-^2)\right] \qquad (9)$$

where I_+ and I_- are the raising and lowering operators and the eigen values are:

$$E_Q = \frac{e^2qQ}{4I(2I-1)}\left[3m_I^2 - I(I+1)\right]\left(1+\frac{\eta}{3}\right)^{\frac{1}{2}} \qquad (10)$$

where q is the electric field gradient (EFG) at the nucleus and η is the assymmetry parameter:

$$\eta = \frac{V_{xx} - V_{yy}}{V_{zz}} \qquad (11)$$

V_{xx}, V_{yy}, V_{zz} are the three components of the EFG tensor and are usually choosen so that $|V_{zz}| \geq |V_{xx}| \geq |V_{yy}|$ making $0 \leq \eta \leq 1$. In Eq.10 only square of m_I occurs which shows that energy levels with m_I differing only in sign are degenerate. Thus for Fe^{57}, only the excited state I = 3/2 gets split into two levels and we get a two line quadrupole split spectra.

The higher order terms are not significant. The investigation of the above interactions helps to understand the structural aspects of compounds. We treat these interactions separately below:

(a) Isomer Shift

It was first reported by Kistner and Sunyar[24] who noticed that the position of the resonance line from a given single line source depends on the chemical form of a single absorber. It may be readily understood in the following way: The nuclear excited and ground states have different effective charge radii, and the electrostatic interaction between (atomic) electrons and the nuclear charge is different for the ground and excited states, Thus the energy of the transition is effected by the electronic charge density at the nucleus (due to atomic s-electrons) and hence by the chemical environment(Fig.2). The analogous energy shift appears in atomic hyperfine

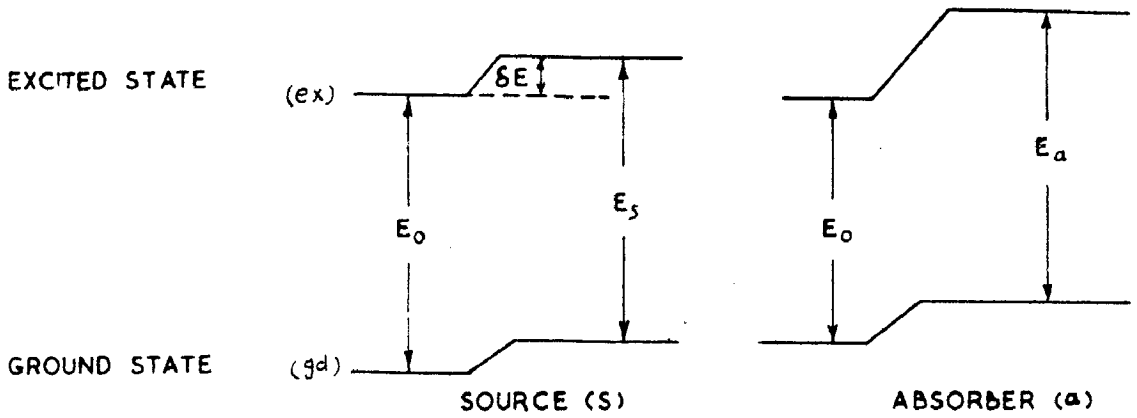

$$\delta E = \frac{2\pi}{5} Ze^2 \left(\Psi(0)\right)^2 R^2 \quad \text{(RELATIVE TO POINT NUCLEUS)}$$

$$E_s = E_0 + \frac{2\pi}{5} Ze^2 |\psi_s(0)|^2 \left[Rex^2 - Rgd^2\right]$$

$$E_s = E_0 + \frac{2\pi}{5} Ze^2 |\psi_a(0)|^2 \left[Rex^2 - Rgd^2\right]$$

ISOMER SHIFT $= E_a - E_s$

$$\text{I.S.} = \frac{2\pi}{5} Ze^2 \left[|\psi_a(0)|^2 - |\psi_s(0)|^2\right]\left[Rex^2 - Rgd^2\right]$$

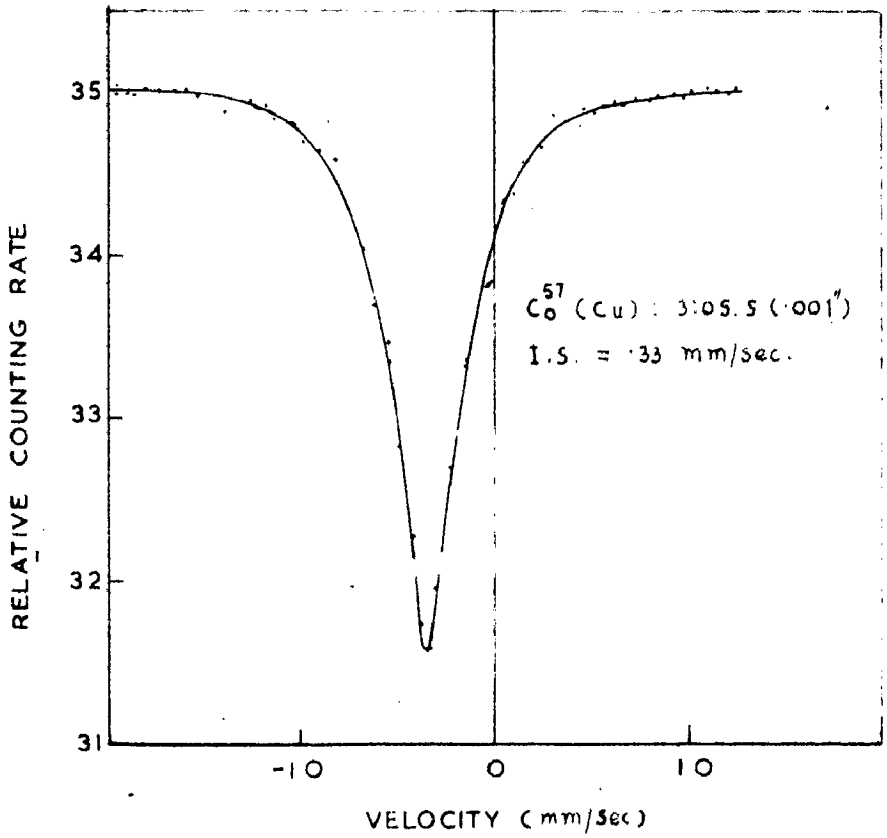

FIG. 2 ISOMER SHIFT. THE EFFECT OF ELECTRIC MONOPOLE INTERACTION IS TO SHIFT NUCLEAR LEVELS WITHOUT LIFTING THE SPIN DEGENERACY.

levels[25] and has been observed in Hg^{197}. Experimentally observed quantity is the difference between the transition energies in the emitter and absorber and for a non-relativistic case is given in Eq.6 for a uniform charge distribution through-out the nucleus (assumed to be spherical). Relativistic Eq. was given by Shirley[26] and is based on Dirac's equation for an atom in a coulombic field. The electron density near the nucleus P(r) is:

$$P(r) = \frac{2(1+\rho)\,|\psi(0)|^2}{r^2(2\rho+1)}\, y^{(2\rho-2)} \qquad (12)$$

where $y = \frac{2Zr}{a_0}$; and $\rho = (1+\alpha^2 Z^2)$. Here $|\psi(0)|^2$ is the non-relativistic electron density. As Z approaches zero, for light elements, ρ approaches 1 and P(r) approaches $|\psi(0)|^2$.

The perturbation potential is the difference between the potential arising from a uniform charge distribution within the nucleus, $V(r) = \frac{Ze^2}{R}\left[-\frac{3}{2}+\frac{1}{2}\left(\frac{r}{R}\right)^2\right]$ and the potential produced by a point nucleus at origin, $-\frac{Ze^2}{r}$. Integrating the perturbation potential, weighted with P(r) we get:

$$\Delta E = \frac{6\pi R_\infty a_0^3 (1+\rho)\,|\psi(0)|^2\, y_0^{2\rho}}{Z\rho(2\rho+1)(2\rho+3)\,\Gamma^2(2\rho+1)} \qquad (13)$$

where $y = y_0$ for $r = R$. After differentiation and substitution we get

$$I.S. = \left\{ \frac{4\pi Z e^2 R^2}{5 h c} \right\} S(Z) \frac{\delta R}{R} \left[|\psi(0)|^2_{abs.} - |\psi(0)|^2_{source} \right] \qquad (14)$$

where $S(Z) = \dfrac{30(1+\rho)\,\gamma_0^{2\rho-2}}{(2\rho+1)(2\rho+3)\,\Gamma^2(2\rho+1)}$ is the relativity factor which approaches 1 as $\rho \rightarrow 1$ for low Z.

Eq.14 consists of two factors: the first contains only nuclear parameters, in particular the difference between the radii of the excited and ground state; the second factor contains the electronic charge density at the nucleus which is basically an atomic or chemical parameter. The sign of I.S. depends on the sign of δR which need not to be positive. Indeed it is negative for Fe^{57} i.e. the excited state has a smaller radius than the ground state. Furthermore, the I.S. is proportional to $|\psi(0)|^2$ i.e. the s-electron density at the nucleus.

Several Mössbauer experiments on iron compounds show characteristic values for I.S. in di-and trivalent states. It may seem strange at first site because the atomic configuration of these two differ only by a 3d electron ($3d^6$ for Fe^{2+} and $3d^5$ for Fe^{3+}) which does not contribute noticeably to $|\psi(0)|^2$. However the effect on I.S. arises indirectly via 3s-electrons which spend a fraction of their time further from the nucleus than 3d electrons. The electrostatic potential which they experience there depends on the screening effects of inner

electrons. Thus adding a 3d electron reduces the attractive Coulomb potential and causes the 3s electron wavefunction to expand reducing its charge density at the nucleus. In this way the addition of sixth 3d electron (in going from Fe^{3+} to Fe^{2+}) reduces the charge density at the nucleus and so is responsible for the positive I.S. Hartree Fock[27] calculations for various configurations of multiply ionized free iron ion can be used to determine the value of the chemical parameter if we assume that the electronic charge density in an ionic salt is the same as in free ion.

The case of covalent complexes is relatively more complex. We should take the relative importance of s, p and d wavefunctions in bonding as well as the extent to which the d electrons are delocalized to the ligands. The d electron contribution can be determined by Hartree Fock calculations, and for s electrons Fermi-Segre-Goudsmit formula[28] can provide the $|\psi(o)|^2$ contribution, this is opposite to the effect of d electrons. The contribution due to p electrons should be very small. Experimentally it has been found that the more covelent of the di-and trivalent compounds have a smaller I.S. than ionic ones i.e. the effect of s electron augmentation is greater than that of d electron augmentation with an exception of hexavalent iron (K_2FeO_4).[29] The shifts show the following sequence in its value for the spin paired and spin free compounds:

$Fe^{2+}_{\text{spin free}} > Fe^{3+}_{\text{spin free}} > Fe^{2+}_{\text{spin paired}} > Fe^{3+}_{\text{spin paired}}$

(b) Quadrupole Splitting

If the nucleus does not have spherical symmetry (as has been assumed in the description of I.S.) it will posses nuclear quadrupole moment, Q. An oblate (flattened) nucleus has a negative quadrupole moment while a prolate (enlongated) one has a positive moment. The interaction of this moment with the gradient of the electric field is called the quadrupole interaction. The energy levels are given in Eq.10. If the crystal has an axis of symmetry (say, the z-axis) then $\eta = 0$. In this case the sublevels are designated by m ($= I_z$), and the quadrupole energy shift for the 14.4 keV level of Fe^{57} (with I = 3/2) is given by:

$$E_Q = \frac{e^2qQ}{12}\left(3m_I^2 - \frac{15}{4}\right) \qquad (15)$$

Thus the $m = \pm 3/2$ states are raised by an energy $E_Q = \frac{e^2qQ}{4}$, and the $m = \pm 1/2$ states are lowered by the same energy. This together with the isomer shift is depicted in Fig.3.

The measurement of the quadrupole coupling e^2qQ unfortunately givesonly the product of Q and EFG. To obtain a valuable test of nuclear models, requires an independent evaluation of the EFG tensor. There are two fundamental sources of the origin of the EFG, the charge on distant ions and the electrons in incompletely filled shells of the atom

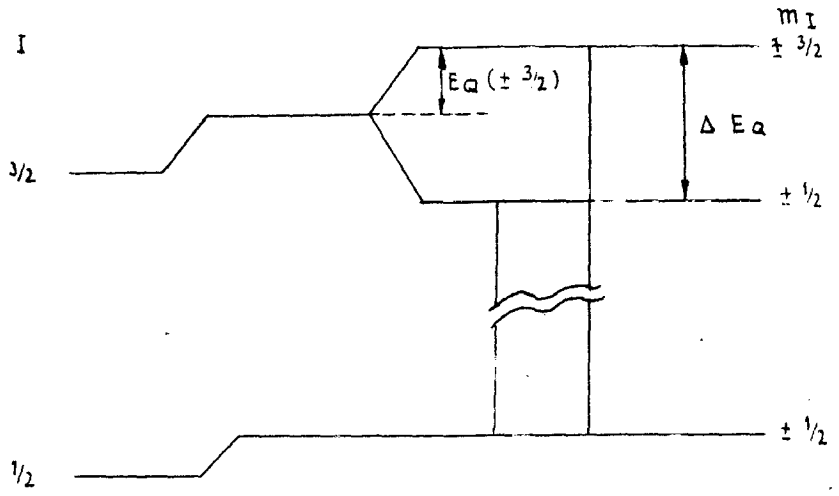

ISOMER SHIFT QUADRUPOLE SPLITTING

$$E_Q(m_I) = e^2 q Q \left[\frac{3m_I^2 - I(I+1)}{4I(2I-1)} \right]$$

$$\Delta E_Q = E_Q(3/2) - E_Q(1/2) = \frac{e^2 q Q}{2}$$

FIG. 3. QUADRUPOLE SPLITTING IN Fe^{57}.

itself (for details refer to chap.IV). Interaction of the partly filled d orbitals with the filled shell of the iron core can also produce a gradient at the nucleus. Even with a symmetrical charge distribution, as in the case of $3d^5$ state of Fe^{3+} there exists an electric field gradient and this could be attributed to the spin-spin interaction of the d electrons with the ligand field. For iron coordination compounds one would expect to find the maximum quadrupole splitting in high spin $3d^6$ configuration of iron with the low spin $3d^5$ next. The high spin $3d^5$, and low spin $3d^6$ produce very small ΔE_Q[30]. A correlation between the magnetic susceptibility and electric quadrupole splitting has been found by Duncan[30] and Nicholson[31].

Other than the position of the quadrupole lines, the intensities of these two lines are also useful which contain additional information. The relative transition probabilities and angular intensity dependence of the two quadrupole lines for I = 3/2 to I = 1/2 transition are tabulated below:

Transition	Relative Transition Probability	Angular Dependence
$\pm 3/2 \longrightarrow \pm 1/2$	1	$\frac{3}{2}(1+\cos^2\theta)f(\theta)$
$\pm 1/2 \longrightarrow \pm 1/2$	1	$(1+\frac{3}{2}\sin^2\theta)f(\theta)$

where θ is the angle from the axis of highest symmetry.

The ratio of intensities of the two lines in the absorption spectra, assuming isotropy of recoilless emission, is:

$$\frac{I_3(\pm\frac{3}{2} \longrightarrow \pm\frac{1}{2})}{I_1(\pm\frac{1}{2} \longrightarrow \pm\frac{1}{2})} = \frac{3(1+\cos^2\theta)}{(2+3\sin^2\theta)} \qquad (16)$$

For a polycrystalline sample, $\overline{\cos^2\theta} = 1/3$, $\overline{\sin^2\theta} = 2/3$, the ratio of $\frac{I_3}{I_1} = 1$. But for a single crystal absorber the ratio of intensities is dependent on angle θ . However when f is anisotropic, the intensities of the two lines are not equal even for a polycrystalline sample[32]. The anisotropy in f have been observed in various tin-organic compounds[33].

(c) Magnetic Dipole Splitting

The magnetic interaction between the dipole moment of a nucleus and a magnetic field due to atom's own electrons has been known through the study of optical hyperfine structure. Until the discovery of Mössbauer effect this interaction could be observed only by its effects on the energy of the electronic transitions. Mössbauer techniques made it possible to be observed in the resonance spectrum of γ-rays emitted and absorbed without recoil. This is the nuclear analogue of the optical Zeeman effect.

The magnetic field, $\vec{H}$, removes the degeneracy of the excited and ground state and splits them each into 2I+1 components. The selection rule for magnetic (or electric)

dipole transition is $\Delta m = \pm 1, 0$, and the Mössbauer spectrum splits into six components separated by an energy $\Delta E = g\mu_n H$, when there is no nuclear relaxation. The relative energies of these transitions are given by[34,35]

$$|\langle I_g m_g LM | I_e m_e \rangle|^2 \quad F_L^M(\theta)$$

where the first factor is the square of the Clebsch Gordan coefficients describing the vector coupling of I_g and I_e through the radiation field LM, and θ is the angle between the direction $\vec{H}$ and the incident γ-rays, the radiation pattern for dipole radiation $F_L^M(\theta)$ is:

$$F_1^0(\theta) = 3/2 \sin^2\theta$$

$$F_1^{\pm 1}(\theta) = 3/4 (1+ \cos^2\theta)$$

For Fe^{57}, where $I_e = 3/2$, $I_g = 1/2$, $L = 1$, and the relative probabilities for various allowed transitions are given in table I.

TABLE I

Relative probabilities for various allowed transition in Fe^{57}

Transition	Δm	Total	Angular Dependence
$3/2 \rightarrow 1/2$	-1	3	$9/4(1+\cos^2\theta)$
$-3/2 \rightarrow -1/2$	+1		
$1/2 \rightarrow 1/2$	0	2	$3\sin^2\theta$
$-1/2 \rightarrow -1/2$	0		
$-1/2 \rightarrow 1/2$	+1	1	$3/4(1+\cos^2\theta)$
$1/2 \rightarrow -1/2$	-1		

For radom orientation of $\bar{H}$ with respect to the γ-ray direction, the radiation is unpolarized and the lines have intensities in the ratio 3:2:1:1:2:3. For $\theta = 90^{o}$, the ratios are 3:4:1:1:4:3 with linear polarization $\parallel, \perp, \parallel, \parallel, \perp, \parallel$. For $\theta = 0$, the radiation is circularly polarized with $\Delta m = 0$ transition missing and the remaining four lines have intensities 3:1:1:3 with polarizations left, right, left, right.

Using a single line Co^{57} in Cu source and a natural iron metal absorber, Fig.5, shows a Mössbauer hyperfine spectrum of the 14.4 keV transition in Fe^{57}. This spectrum has been used extensively[36] and was the first γ-ray hyperfine spectrum reported[37]. From the energy level diagram, Fig.4, it can be seen that the six fingured pattern is sufficient to determine the ratio of the excited and ground state magnetic moments as well as the value of the internal magnetic field $\bar{H}$.

2. LIGAND FIELD THEORY OF A 3d ION IN A FIELD OF OCTAHEDRAL SYMMETRY

Ligand field theory which contains as limiting cases the crystal field theory of "ionic" complexes and the molecular orbital theory of strongly bound "covalent" complexes has been developed as a means of calculating the wavefunction and energy levels for atoms in complexes. We will be concerned with its application to complexes of atoms or ions which possess incomplete d shells(metals of the transition series of the periodic table). In the case of a free atom a set of

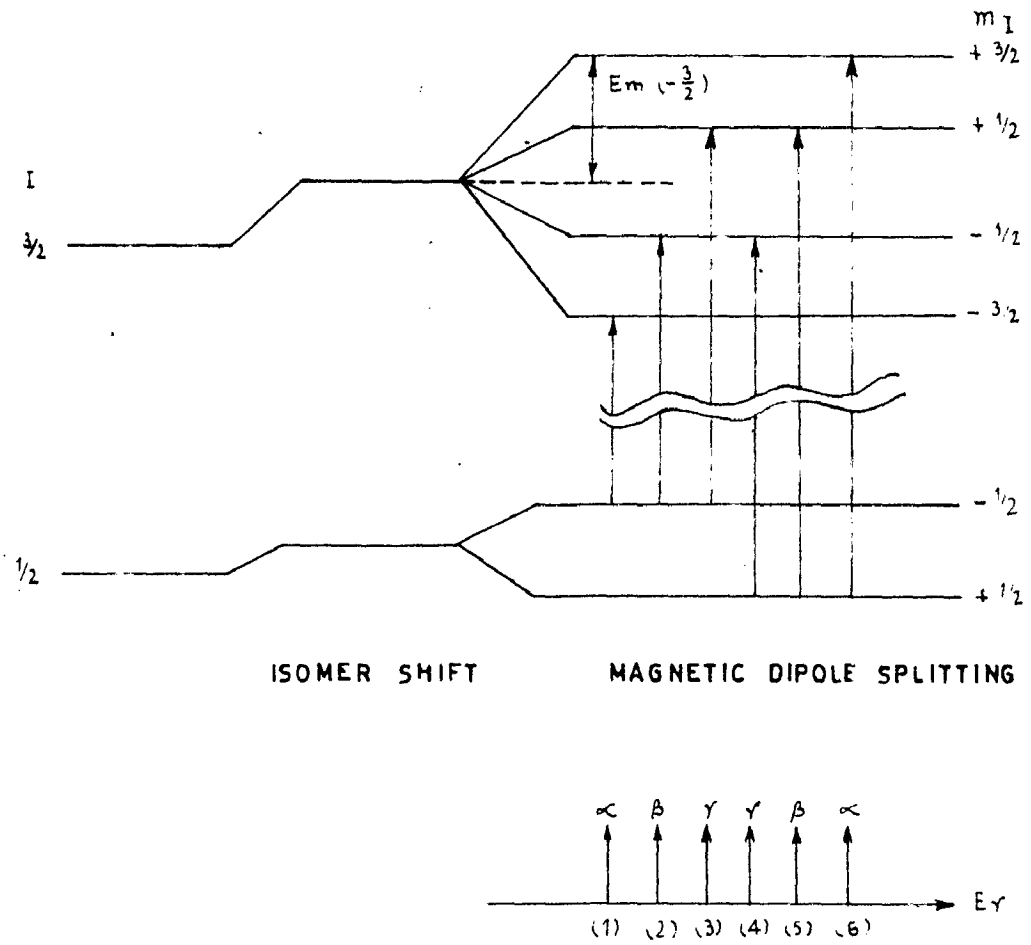

FIG.4. MAGNETIC HYPERFINE STRCTURE OF THE 14·4 keV TRANSITION IN Fe^{57}.

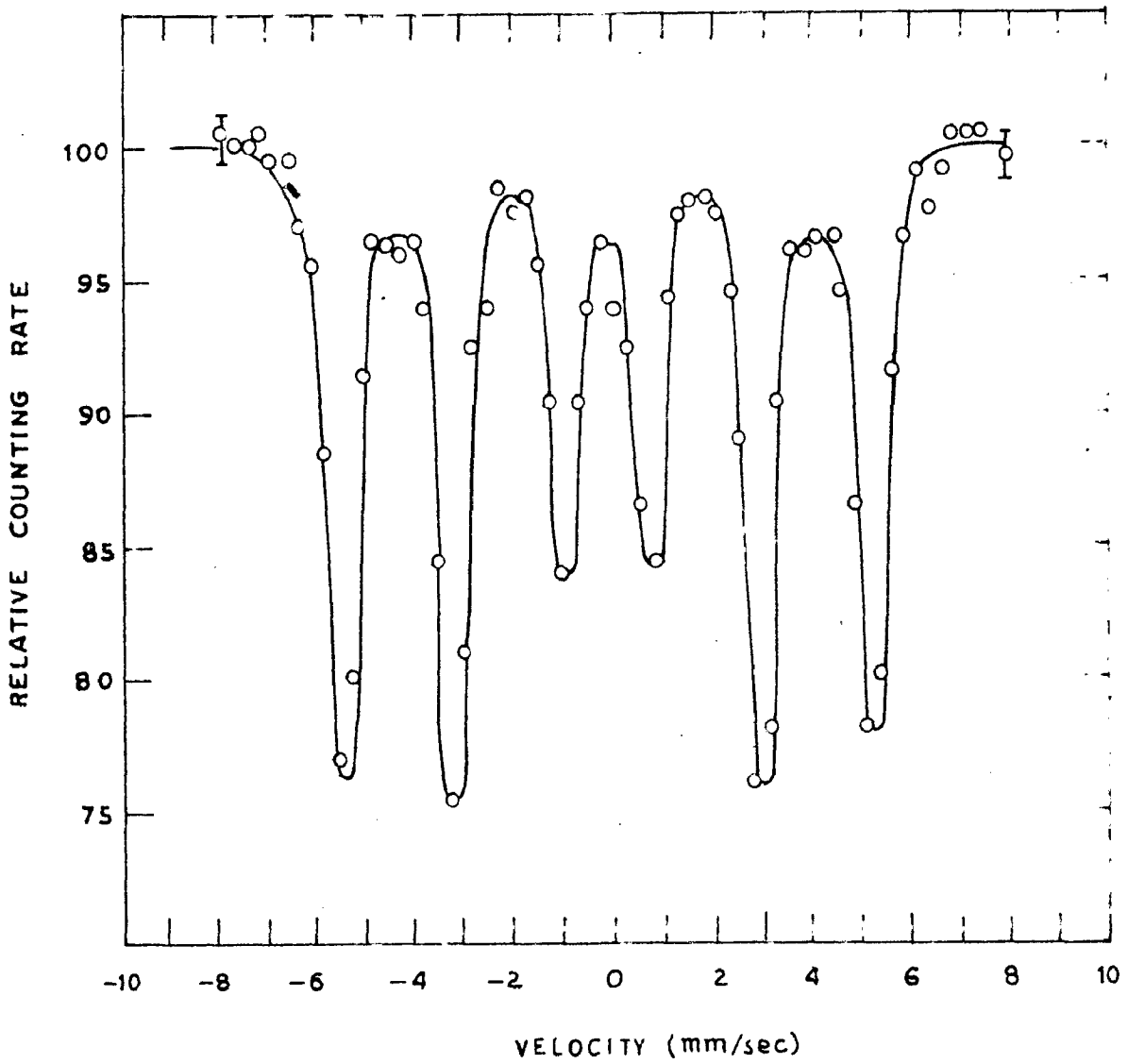

FIG. 5. MÖSSBAUER ABSORPTION SPECTRUM OF Fe^{57} IN METALLIC IRON SHOWING THE MAGNETIC HYPERFINE STRUCTURE.

five d orbitals is perfectly degenerate but in a complex these sets of orbitals are obliged to split into smaller sets, each of which transforms according to irreducible representation of the point group of the complex. The complexes we are concerned with, belong to the octahedral point group O_h, for which the largest irreducible representations are of dimension 3, so no energy level in such a complex can be more than three-fold degenerate. The various sets of orbitals differ in their energy of interaction with the field of the ligands and it is our purpose to determine the splitting of orbital degeneracy in the presence of an octahedral ligand field e.g. in $[Fe(CN)_6]^{4-}$ and $[Fe(H_2O)_6]^{2+}$ ions.

The Hamiltonian operator for an atom in a complex is

$$\mathcal{H} = -\frac{\hbar^2}{2m}\sum_j \nabla_j^2 - \sum_j \frac{Z_j e^2}{r_j} + \sum_{j>k} \frac{e^2}{r_{jk}} + \sum_j \zeta_j \, l_j \cdot s_j + V \qquad (17)$$

which is identical, except for the last term, with the Hamiltonian for a free atom. The term V represents the energy of interaction with the ligands. The three different limiting cases which depend on the relative magnitudes of V and other two terms are as follows:

(i) $V < \sum_j \zeta_j \, l_j \cdot s_j$	Complexes of the rare earths
(ii) $\sum_{j>k} \frac{e^2}{r_{jk}} > V > \sum_j \zeta_j \, l_j \cdot s_j$	Complexes of the first transition series. Weak field cases.
(iii) $V > \sum_{j>k} \frac{e^2}{r_{jk}}$	"Covalent" complexes. Strong field cases

It is convenient to expand V in a series of normalized spherical harmonics:

$$V = \sum_i \sum_l \sum_m Y_l^m(\theta_i, \phi_i)\, R_{nl}(r_i) \qquad (18)$$

where the first summation is over the i electrons of the cation. It is imperative to know the symmetry of ligands around the cation, because V must transform as the totally symmetric representation in the symmetry representation of the molecule. The term corresponding to $l = 0$ in Eq.18 has spherical symmetry and is given by

$$V_R = \sum_i \frac{1}{\sqrt{4\pi}} R_o(r_i) \qquad (19)$$

This term although responsible for the major part of lattice energy of a crystal or heat of solution of a cation, has no effect on the electronic properties of the molecule, since it causes a uniform downward shift of all levels with the same number of electrons, without removing any degeneracies or altering the overall pattern.

The potential V may be separated into a spherically symmetrical part V_R and a part V_o which has the symmetry of the arrangement of ligands. We consider the effect of an octahedral field on a set of five degenerate d orbitals. The point group O is comprised of the operations of pure rotations E, C_2, C_3 and C_4 and the complete octahedral point group O_h is obtained by adding the operation of

inversion, i, to these operations. This results only in doubling the number of irreducible representations since each representation of O has the possibility of being symmetric or antisymmetric (g or u) with respect to the operation of inversion in the center of symmetry. However we will deal with O rather than with O_h.

The d-orbital functions are of the form

$$\psi = R(r)\, Y_\ell^m(\theta,\phi) \tag{20}$$

$$Y_\ell^m = P_\ell^m(\cos\theta)\,\frac{e^{im\phi}}{\sqrt{2\pi}} \tag{21}$$

and m has the values 2,1,0,-1,-2.

Defining that $\bar{Z}$-axis of the atom as the axis about which the rotations are carried out, we learn that $P_1^m(\cos\theta)$ is invarient with respect to rotations about this axis. Furthermore the radial function R is invarient under all operations of a point group. Thus the effect of rotation by an angle α about the $\bar{Z}$-axis is to change $e^{im\phi}$ to $e^{im(\phi+\alpha)}$ and expressing this result in matrix form, we get

$$\begin{pmatrix} e^{2i(\phi+\alpha)} \\ e^{i(\phi+\alpha)} \\ e^{0} \\ e^{-i(\phi+\alpha)} \\ e^{-2i(\phi+\alpha)} \end{pmatrix} = \begin{pmatrix} e^{2i\alpha} & 0 & 0 & 0 & 0 \\ 0 & e^{i\alpha} & 0 & 0 & 0 \\ 0 & 0 & e^{0} & 0 & 0 \\ 0 & 0 & 0 & e^{-i\alpha} & 0 \\ 0 & 0 & 0 & 0 & e^{-2i\alpha} \end{pmatrix} \begin{pmatrix} e^{2i\phi} \\ e^{i\phi} \\ e^{0} \\ e^{-i\phi} \\ e^{-2i\phi} \end{pmatrix} \tag{22}$$

The character of the operation is given by the trace

of the transformation matrix and is

$$\chi(\alpha) = e^{2i\alpha} + e^{i\alpha} + e^{0} + e^{-i\alpha} + e^{-2i\alpha}$$
$$= 2\cos 2\alpha + 2\cos\alpha + 1 \qquad (23)$$

Now α is equal to 0, π, $\frac{2\pi}{3}$ and $\frac{\pi}{2}$ for $E, C_2 C_3$ and C_4 respectively, hence

$$\chi(E) = 5$$
$$\chi(C_2) = 1$$
$$\chi(C_3) = -1 \qquad (24)$$
$$\chi(C_4) = -1$$

Since the spherical harmonics of order L form a basis for representing the group of all rotations, they definitely do so for the finite group of rotations O. To examine whether we can reduce the representation into smaller irreducible ones for this smaller group, we require the character of D_2 together with the decomposition formula. Table II gives the character table of O.

TABLE II

The character table of irreducible representation of O point group.

O	E	$8C_3$	$3C_2$	$6C_2$	$6C_4$
A_1	1	1	1	1	1
A_2	1	1	1	-1	-1
E	2	-1	2	0	0
T_1	3	0	-1	-1	1
T_2	3	0	-1	1	-1

For convenience, the characters of the reducible representations of O,Eq.24,for point group O are tabulated below in Table III.

TABLE III

Character table of group O

O	E	$8C_3$	$3C_2$	$6C_2$	$6C_4$
D_2	5	-1	1	1	-1

We learn by inspection that the rows E and T_2 in Table II should be added together to produce the row D_2 in Table III. Hence we have that a D state is split into a two-fold and a three-fold degenerate level in a cubic field which transform according to the e_g and t_{2g} representations respectively;

$$D_2 = e_g + t_{2g} \tag{25}$$

where small letters are customarily used for the representation to show that they arise from one-electron orbitals (s,p,d,....)rather than from atomic terms (S,P,D,....) and the g (gerald) subscript is added, to show that these refer to the even parity case. The angular dependence of the ferrous or ferric ion orbital wavefunctions corresponding to each energy level E and T_2 is tabulated in Table IV.

TABLE IV

Angular dependence of orbital wavefunctions for octahedral symmetry (O) classified according to their transformation properties[38].

Irreducible representation (energy level label)	Spherical harmonic form	Cartesian coordinate form
E	$\lvert Y_2^0 \rangle$	$\lvert 3z^2 - r^2 \rangle$
	$\frac{1}{\sqrt{2}} \lvert Y_2^2 + Y_2^{-2} \rangle$	$\lvert x^2 - y^2 \rangle$
T_2	$\frac{1}{\sqrt{2}} \lvert Y_2^1 + Y_2^{-1} \rangle$	$\lvert zy \rangle$
	$-\frac{i}{\sqrt{2}} \lvert Y_2^2 - Y_2^{-2} \rangle$	$\lvert xy \rangle$
	$-\frac{1}{\sqrt{2}} \lvert Y_2^1 - Y_2^{-1} \rangle$	$\lvert zx \rangle$

Individual d orbitals are labeled d_{xy} d_{yz} d_{xz}, $d_{x^2-y^2}$ and d_{z^2}, indicating that the lobes of maximum electron density lie along the coordinate axes for $d_{x^2-y^2}$ and d_{z^2} and between the axes for the others, Fig.6. The ligands are normally either negative ions or dipolar molecules which are oriented so that the negative pole is directed toward the central cations, hence the energies of d orbitals which point towards the ligands will be increased relative to those which point between the ligands. Therefore $d_{x^2-y^2}$ and d_{z^2} orbitals lie above d_{xy}, d_{yz} and d_{xz} in an octahedral complex. We identify the first two as the components of e_g and the other three as the components of t_{2g} in the point

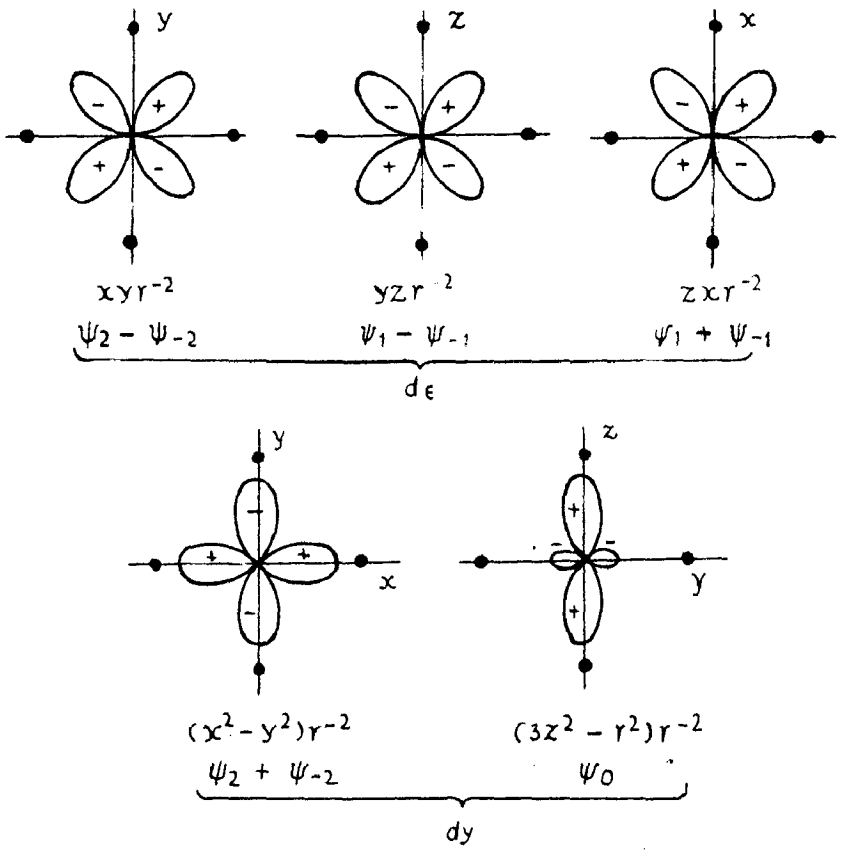

FIG. 6. DIAGRAMS OF d-ELECTRON ORBITALS SITUATED AT A SITE OF OCTAHEDRAL SYMMETRY IN RELATION TO SIX EQUIVALENT POINT CHARGES, SHOWN AS DOTS.

group O (or O_h). The results of splitting of d orbitals are shown in Fig.7. If the environment is distorted from octahedral symmetry, the three-fold degeneracy of t_{2g} and two-fold degeneracy of e_g levels are further lifted.

The magnitude of 10 Dq varies little through the first transition series (e.g. about 10,000 cm^{-1} for the divalent hydrates, about 20,000 cm^{-1} for the trivalent hydrates) but becomes considerably larger in the second and third transition series. Suppose that a Fe^{+++} ion with five 3d electrons is placed in a weak electrostatic field. There is, in effect, a competition between the tendency to keep the energy of the ion low by obeying Hund's Rule and the tendency to put the electrons into the t_{2g} orbitals. If the splitting between the two sets of levels is very small (weak field), the electrons remain unpaired and Hund's Rule is satisfied giving rise to spin-free or high-spin configuration. Whereas in the case of a strong field, the splitting between levels is large, the electrons pair off and are found in the t_{2g} levels, thereby giving rise to spin-paired or low-spin configuration The low polarizability of the F^- ions produces a weak field at the Fe^{3+} ion, whereas the high polarizability of the CN^- ions produces a strong field as shown in Fig.8. The theory successfully explains the observed magnetic moments of the two ions.

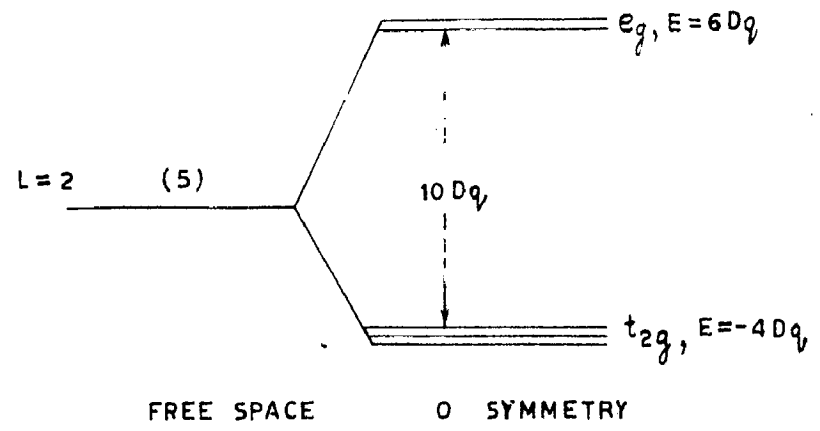

FIG. 7. SPLITTING OF THE α ORBITATS IN AN OCTAHEDRAL FIELD.

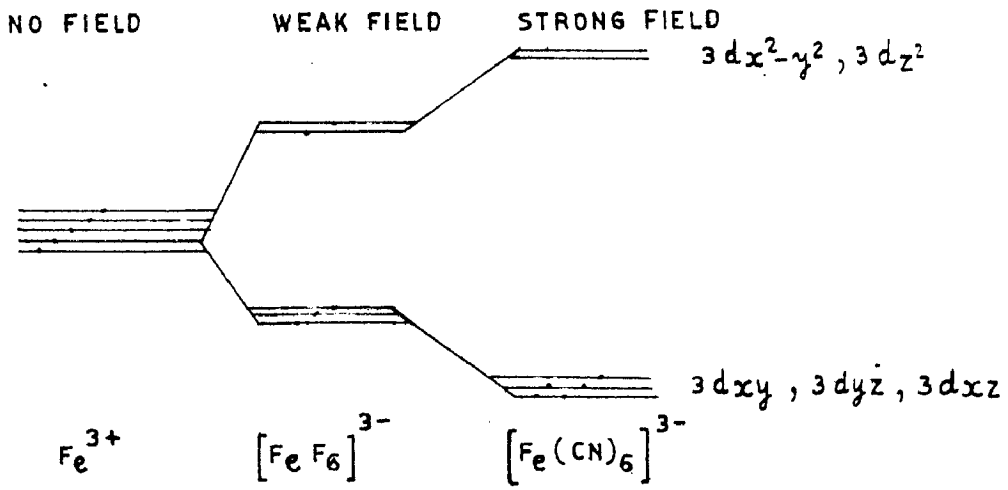

FIG. 8. DISTRIBUTION OF UNPAIRED ELECTRONS IN WEAK AND STRONG CRYSTAL FIELDS.

3. STATEMENT OF THE PROBLEM

The intent of the experimental investigations reported in the succeeding chapters of the thesis has been two fold:

(i) Firstly to use Mossbauer effect for a systematic investigation of the ferro- and ferricyanide super complexes formed by replacing the cation in the potassium ferro- and ferricyanide complexes by 3d transition elements; Cr, Mn, Fe, Ni, Co, Cu and Zn. Since such a study is expected to provide

(a) Unambiguous evidence for the change of coordination number of Fe atom

(b) The I.S. values will provide a sensitive test for the validity of the metal-metal charge transfer transition as in the case of Prussian blue and

(c) Furthermore to decide whether the ground state orbital wavefunction is a singlet $3d_{xy}$ or a doublet $3d_{yz}$ and $3d_{xz}$.

(ii) The electric field gradient, EFG, depends on the electronic state of the atom and from the quadrupole split doublet absorption spectrum of single crystal of a paramagnetic salt, one can conclude both the ground state orbital wavefunction and the sign of quadrupole coupling constant; the latter having structural implications. EFG is represented as a traceless symmetric tensor of second rank and is completely specified by five independent parameters.

Single crystals of $Fe(NH_4SO_4)_2 \cdot 6H_2O$ and $FeSO_4 \cdot 7H_2O$ were studied with the following perspective

(a) To locate the principal axes of the EFG relative to the crystal axes

(b) To determine the quadrupole coupling constant

(c) To find the asymmetry parameter

(d) To find whether the principal axes of EFG tensor coincide or not with the principal axes of the susceptibility tensor; and

(e) To find how far anisotropy of Lamb-Mössbauer fraction is effective.

The details of the fabrication, checking and calibration of the requisite instrumentation constitute the subject matter of chapter II, whereas the observations, analysis and discussion in connection with the above cited problems comprise chapters III and IV.

C H A P T E R II

INSTRUMENTATION AND EXPERIMENTAL TECHNIQUE

1. MÖSSBAUER SPECTROMETER

As seen in chapter I, the natural resonance width of a Mössbauer γ-ray is extremely small ($\sim 1 \times 10^{-8}$ eV for 14.4 keV γ-ray of Fe^{57}). For resonance absorption to occur, normally it is essential that the chemical environments of the source and absorber are identical, since otherwise small differences either in bonding or nature of ligands of the Mössbauer nucleus will destroy the resonance effect due to shift in its nuclear levels. For instance in his original historic investigations[3], R.L. Mossbauer, made use of Doppler tuning for matching the energy levels of 129 keV γ-ray of Ir^{191} in order to observe the phenomenon of recoilless nuclear absorption. When a source is moved with a linear velocity v with respect to the absorber, the γ-ray suffers a shift in its energy E, called Doppler shift ΔE :

$$\Delta E = \frac{v}{c} E$$

The velocity is defined as positive if the source moves towards the absorber and vica versa. For Fe^{57}, the fractional shift in energy, $\frac{\Delta E}{E} = \frac{\Gamma}{E} = 3.3 \times 10^{-13}$ and for causing such a shift it requires a velocity $v \sim 0.1$ mm/sec. Thus relatively low velocities are needed for these experiments.

A Mössbauer spectrum thus consists of a plot of resonantly absorbed (or scattered) γ-ray intensity as a function of relative velocity between the source and absorber. A Mössbauer spectrometer, therefore, must be capable of providing this relative velocity and at the same time sensing the γ-ray intensity at each value of relative velocity. There are two basic classes of the devices that produce Doppler motion, one having a constant, and the other having a variable rate of motion. The latter devices[39-43] are most videly used because of being un-effected by small changes in the gross counting rate of the gamma ray pulses due to the line voltage fluctuations, detector and amplifier drifts etc..

A signal generator produces a linear increase in voltage with time. This voltage is transformed into velocity in the transducer providing constant accelaration. For stability a feedback arrangement is incorporated in these systems and this in turn is generated from another velocity sensing transducer. The feedback arrangement is particularly called for reducing extranuous motion due to building vibrations, microphonics etc. etc. In such a set-up employing a multichannel analyser a single run gives the entire Mössbauer spectrum. Depending upon the number n of channels in the analyser each period T of the velocity change is divided into n intervals, so that i-th channel of the analyser records the number of counts received in the short period of the time from $t_a = \frac{(i-1)T}{n}$

to $t_b = \frac{iT}{n}$ of each period, which thus correspond to some small range of velocities between $v(t_a)$ and $v(t_b)$.

The other class of velocity drives employ various devices that transform rotational motion (given by the synchronous or D.C. motors) to constant velocity motion.[44-47] Such devices include eccentric cams, linkages, hydraulic pistons, lathes, rotating discs etc. Large masses and powerful motor drives may be used to ensure reasonably constant velocities at low vibration levels. Data are accumulated point by point at each velocity setting. The accuracy of average velocity calibration per cycle is limited, in principle, only by the accuracy in measurements of the distance between gated part of the motion and its time interval.

A constant accelaration drive requires a multichannel analyser and other expensive equipment.. These are not very well suited when one is looking for small shifts in the position of resonance line or when only a small portion of the spectrum is to be scanned. Due to ease of simplicity of fabrication and the non-availability of a multichannel analyser, we decided to employ a constant velocity drive.

(i) Constant Velocity Drive

Schematic sketch of top plane of the drive is shown in Fig.9. We discuss below the salient features which required careful attention for satisfactory operation.

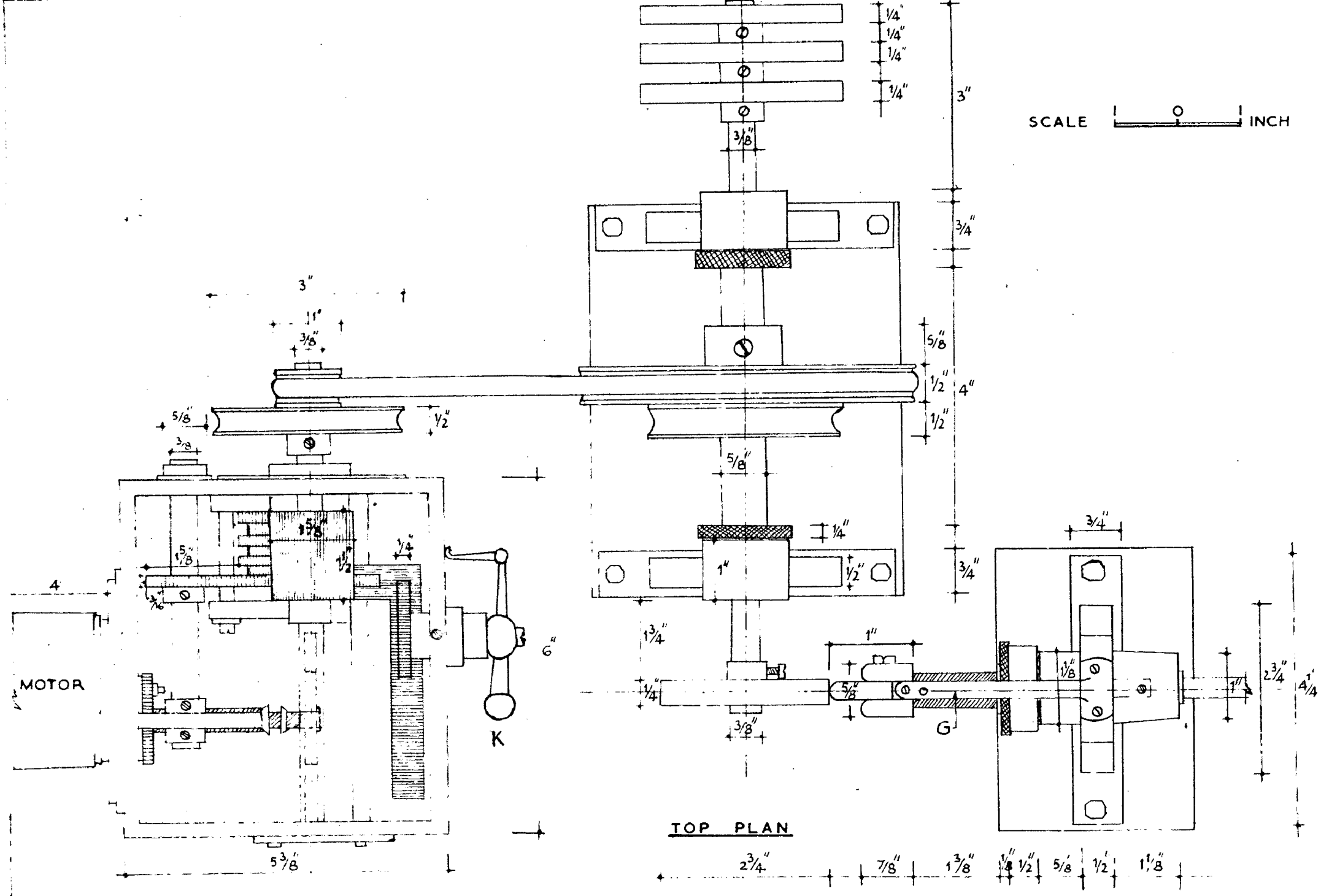

FIG. 9 TOP PLAN OF THE CONSTANT VELOCITY DRIVE.

(a) Constant Velocity Cam

Eccentric cam is used for converting the angular motion to the rectilinear motion. The shape of the constant velocity cam obeys the curve $r = a\theta$. Cutting the profile with an accuracy better than 10^{-3} cm/degree was experienced to be quite difficult. A cam cutting jig was designed as suggested by Mössbauer[13] and its plan is shown in Fig.10. The diameter of the rollers is choosen according to the total lift required (circumference of the roller is twice the lift of the cam). Six strong springs are used to make the tension greater than the grinding force to avoid slipping while cutting. Preshaped cam of ebonite (this material was choosen as it requires lesser grinding force) is tightened on one roller and the handle is rotated slowly. Thus as the cam goes forward the grinder cuts the cam according to the shape desired. It may be remarked that this machine does not necessiate the constant speed of the handle. Having cut half the cam it is inverted and the remaining half portion was ground. The profile is finally dressed with a 300 mesh emery paper in order to make it super smooth.

The checking of the profile is done by mounting the cam on a shaft and noting the lift per degree with a dial guage (least count 0.002 mm). After a number of attempts we succeeded in obtaining a profile of accuracy better than 10^{-3} cm/degree. In order to avoid the instantaneous jerks at the two inflection points of the profile these were

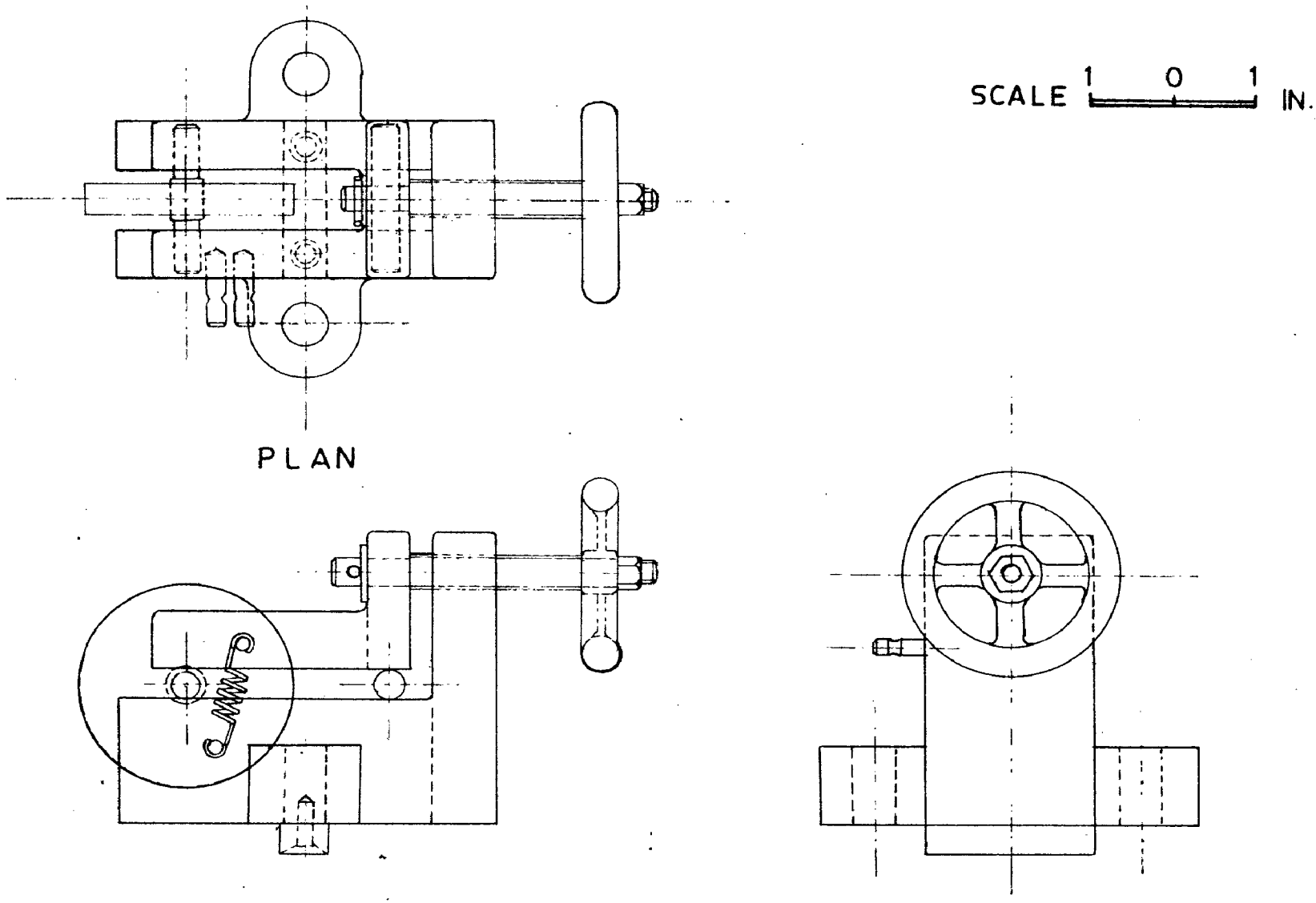

FIG. 10. CONSTANT VELOCITY CAM CUTTING JIG.

ground smooth.

(b) Motor and Gear Box

A small Dynamotor DM-53-AZ manufactured by General Electric Company, U.S.A. is used. It operates at 12 volts and 2,8 amp. and has 6000 rpm. A cabinet of Lead Accumulators was employed to supply a constant input voltage of 12V. The change of input voltage from 5V to 12V could effect the change in speed of the motor from 2000 to 6000 rpm. The speed is reduced by fine toothed gears, with a worm gear at the first stage (speed reduced to 60 rpm) and then by four sets of spur gears in steps of 1:2:5. The master gear attached with the main shaft can be connected with any of the set's gears with the help of a control knob K.'O' ring belt is used for coupling the output with the cam and follower assembly. Considerable care is taken in reducing the jerks and vibrations arising from the gears. A special grease H (Esso) was found quite suitable for the purpose. The motor and gear box assembly and cam and follower arrangement were mounted on separate tables.

(c) Cam and Follower Arrangement

The cam is mounted on a shaft supported by two self aligning double row ball bearings housed in two walls. 'O' ring belt is used for coupling the gear box to the cam follower assembly. The follower, which is perpendicular to the shaft moves in a carefully machined perspex sleeve which provides the smooth motion of the follower. At the

other end of the follower is fixed a Teflon bearing which is kept in contact with the cam by means of type writer springs. The guide G eliminates the possibility of rotation of the follower. Lubrication of the assembly was done with oil 3 in 1.

(d) Control Unit

During one complete revolution of the cam the follower moves to and fro at constant speed (giving both-ve and + ve velocities) except at the two extremities. Mercury switches were employed to exclude from the data the transmitted intensity during decelaration and accelaration of the cam. Three perspex discs with platinum wires fixed in a manner that one end of it is slightly outside the disc's surface and the other in contact with the shaft, are mounted on the latter. Out of the three connections which are taken from the mercury cups, two connect on-off switches (on the instrument pannel) to two scalers and timers (called negative and positive scalers and timers) and the third one goes to the grid of the power amplifier. The power amplifier in turn drives the revolution recorder Fig.11. The common terminal connected to shaft is grounded. The level of the mercury and the angular position of the discs require careful adjustment so that pulse counting stops before decelaration sets in and counting starts a little later when the follower has attained the maximum speed. The distances traversed by the follower during the gated parts of the negative and

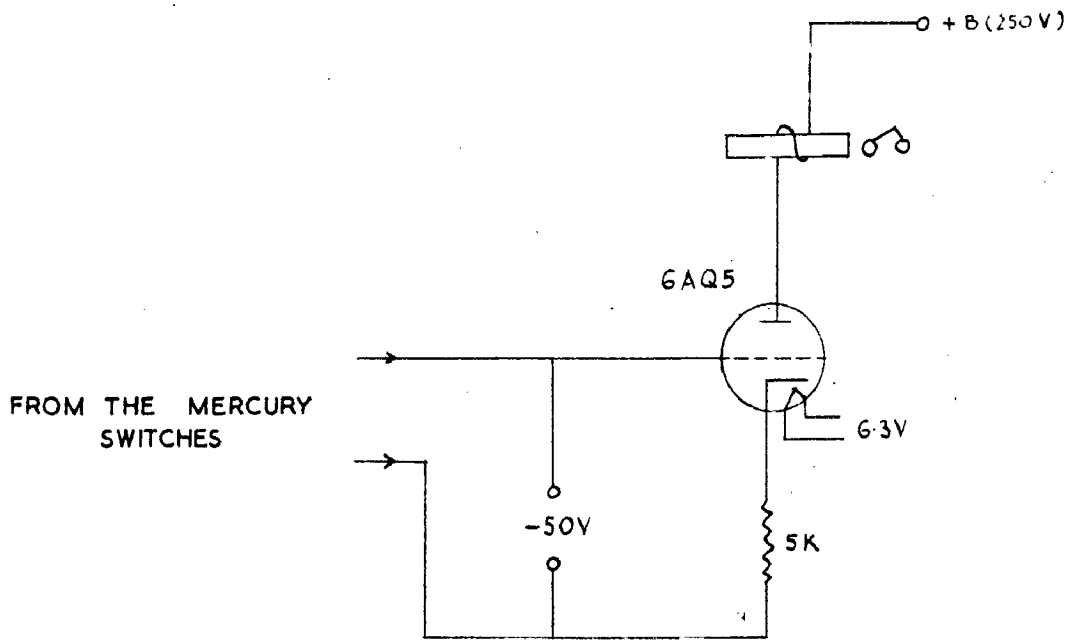

FIG.11. CIRCUIT DIAGRAM FOR THE REVOLUTION COUNTER.

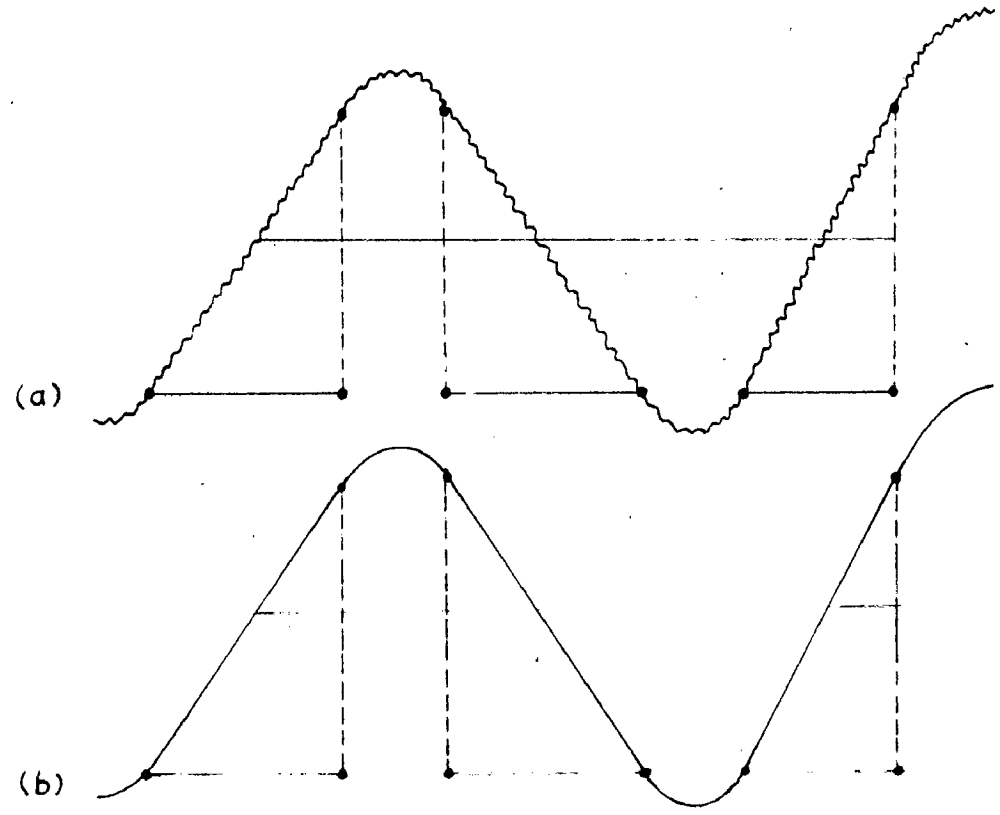

FIG. 12. OSCILLOSCOPIC TRACE OF THE PATH OF THE FOLLOWER (a) VIBRATIONS COUPLED (b) VIBRATION FREE AFTER REPLACING METAL-METAL CONTACT TO METAL-FIBRE CONTACT.

positive motion have been determined with the help of a dial gauge (L.C. = 0.002 mm).

(e) Elimination of Vibrations

The Mossbauer source used in these investigations was initially of activity 1 mC Co^{57} in Cu matrix. Any velocity ripple (vibration) must be kept to a very small fraction of (= 0.1 mm/sec) for making negligible the instrumental broadening. Different parts of the drive are checked regarding its uneven motion and noise of the gears. The final check up is done at the follower stage. A soft iron core is mounted on it which moves in the solenoid having primary and secondary windings. The primary is energised by 10 kc/s simusoidal frequency from an audio oscillator. The induced voltage produced in the secondary due to the motion of the core is fed to the $(YY)_a$ plates of the double beam Cathod Ray Oscilloscope. An artificial pulse is also applied to the $(YY)_b$ plates through the mercury switch which determines the gated portion of the cam during which pulse counting is operative. The shape of the oscilloscopic trace is displayed in Fig.12(a). Having observed all necessary precautions such as alignment, change of metal-metal contact to metal fibre contact etc.; Fig.12(b) shows the final trace. This corresponds to the vibration free motion within the accuracy of the method. To sum up, the following points are considered necessary:

(i) Proper alignment of the shaft carrying the cam, specially the fixing of ball bearings.

(ii) Grease H has been found quite suitable for lubricating the ball bearings and gears. It is viscous enough to damp the noise and uneven motions.

(iii) Metal-fibre contact is preferrable as compared to metal-metal contact. This precaution is particularly important for designing the sleeve and guide for the follower.

(iv) Mounting of cam and follower arrangement on a separate table was insulated from the floor by a cushioning material such as foam rubber.

Despite the above mentioned precautions we did not get as narrow lines in the spectrum of Fe^{57} (Cu) vs Fe metal as are usually obtained with constant accelaration drives at velocities more than 2.5 mm/sec. The cause of this discrepency in the line width could be the lack of absolute constant motion and the stability of electronic circuitry (following section). The specifications of our velocity drive are summarized in Table V.

TABLE V

Specifications of the Mechanical drive used for Doppler tuning the source.

(i) Motion:	Linear constant velocity.
(ii) Velocity:	Variable in the range -12.5 mm/sec to +12.5 mm/sec.
(iii) Length of the stroke: (lift)	Variable from 0 to 4.5 mm.
(iv) Velocity accuracy:	Constant within $\pm$ 0.03 mm/sec, $\pm$0.5% maximum during each stroke.
(v) In put voltage for D.C. motor:	12 VDC at 2.8 amp.

(ii) Electronic Circuitry

In this section we discuss briefly the electronics employed for measuring γ-ray intensity as a function of velocity. As most of these details have become a part of accepted literature, we describe below the arrangement in brief, with emphasis on salient features.

A block diagram of the arrangement is shown in Fig.13. A scintillation head consisting of 1 mm thick NaI(Tl) crystal mounted on RCA 6342 A photomultiplier served as γ-ray detector. The crystals used in conventional γ-ray spectroscopy are 1" thick, these are unsuitable for 14.4 keV γ-ray due to its self-absorption. Moreover such a thickness will degrade the 137 and 123 keV -ray to lower energies through Compton effect so much so that a part of it will be accepted by the Pulse Height Analyser window preset for 14.4 keV γ-ray. Furthermore the associated x-rays of 6.5 keV will not be resolved. The output is fed through the white cathode follower, Fig.14, to the Linear Amplifier and a Single Pulse Height Analyser (model 600B, Eldorado Electronics California) and Decade Scaler (DS 325, Trombay Electronics Division Bombay). For 14.4keV γ-ray energy resolution of 45% was attained. It is comparable to those reported in the literature for NaI(Tl) scintillator of comparable thickness. However this is so much poorer than that for a proportional counter ($\sim$8.5%). The discriminator setting of the P.H.A. was adjusted so that the photopeak corresponding to 14.4 keV energy is selected.

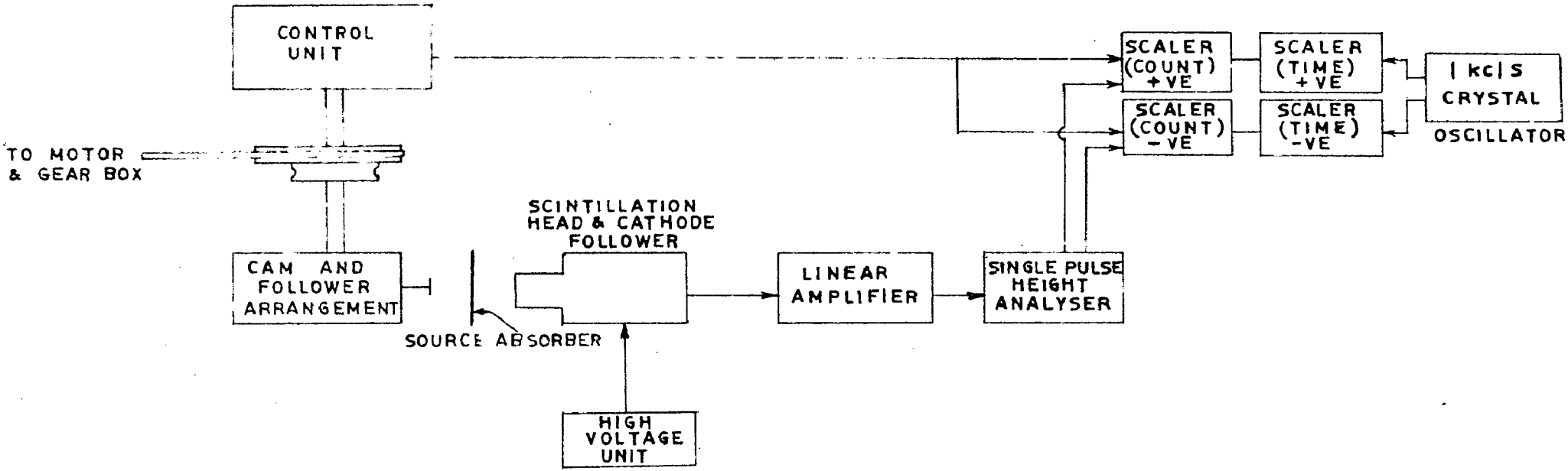

FIG. 13. BLOCK DIAGRAM OF THE RADIATION DETECTION CIRCUITRY.

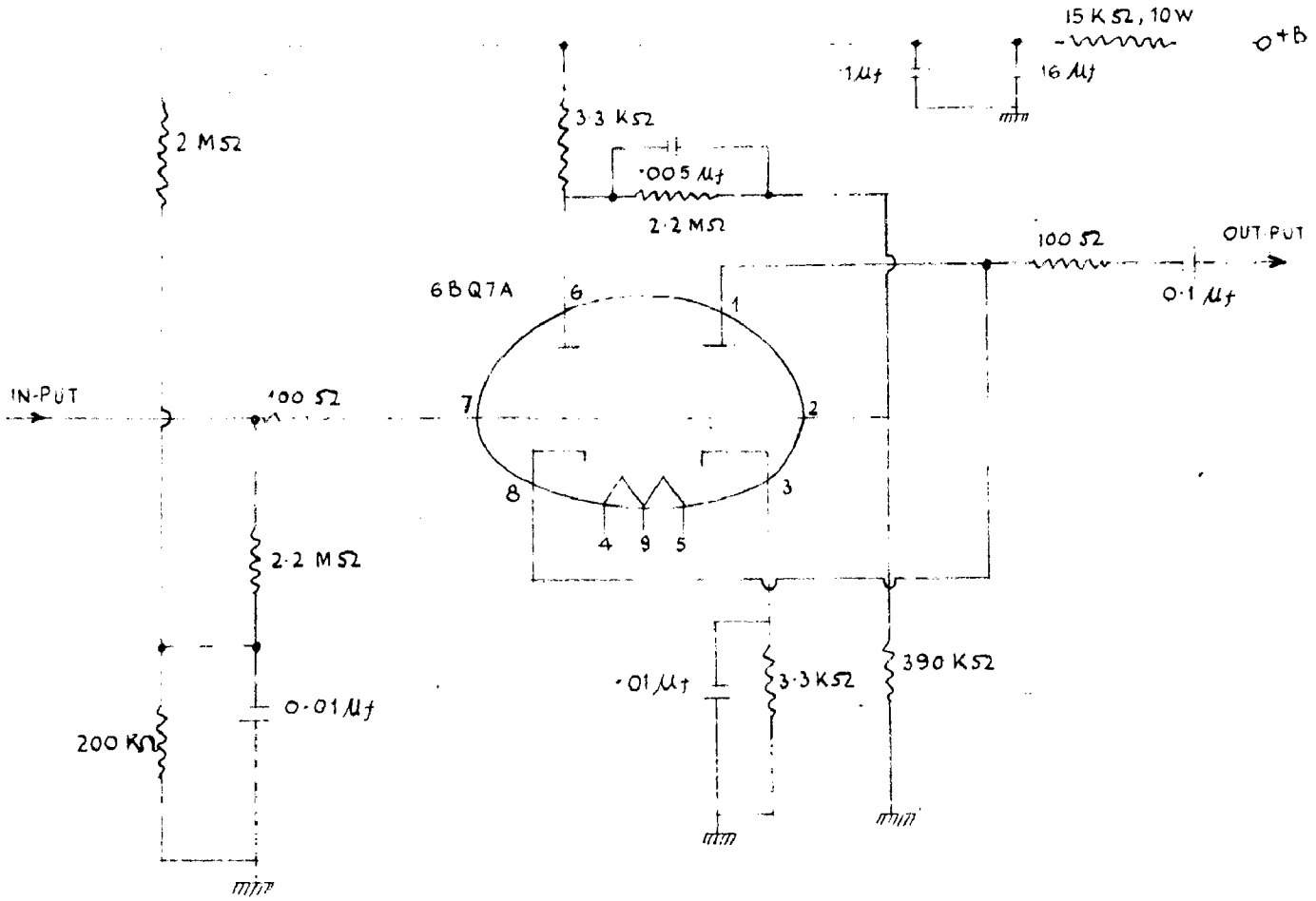

FIG. 14. WHITE CATHODE FOLLOWER.

For completeness, the settings of the amplifier and P.H.A. etc. are: EHT = + 950 V, gain = 1000, channel width = 6 V and threshold = 12.5 V.

The intensities of various energies in the decay spectrum of Co^{57} are $I_{137}:I_{123}:I_{14.4}:I_{x\text{-ray}} \approx 1:10:1:6$. Obviously there is a small overlap of the 14.4 keV γ-rays and 6.5 keV x-rays, while the strong 137 and 123 keV γ-rays are quite outside this region. The 6.5 keV x-ray is suppressed by a 0.001" Al foil on the face of the crystal.

The output from P.H.A. is fed to two scalers simultaneously. These scalers separately store the pulses for the -ve and +ve velocities. Two more scalers are used in the time mode for measuring the time for -ve and +ve velocities. A fixed 1 kc/sec crystal controlled oscillator was used for timing.

Elimination of gain drifts in the electronic circuitry was done by energising this from voltage stablizers in cascade. The input voltage was stable within $\pm$ 1 V.

(iii) Calibration

During the present investigations the source used is Co^{57} in 0.002" Cu matrix of initial activity 1 mC, purchased from Nuclear Science and Engineering Corporation, Pittsburgh Pa, U.S.A. It is mounted in a perspex holder which can easily be screwed with the follower of the velocity drive. Collimation of the γ-ray beam is done by

placing lead bricks with a 1/4" hole. This is considered essential to eliminate the scattered intensity from entering the detector. The absorber under study was placed on a mount consisting of a 1/8" thick lead plate with a 3/4" centre bore. This was placed perpendicular to the direction of γ-rays. The source and detector distance is approximately 5" and the absorber is placed in the middle.

A Mössbauer spectrum consists of a plot of Mössbauer γ-ray intensity as a function of relative velocity between the source and the absorber. Two types of intensity measurements are possible, either of the transmitted or scattered rays. For scattering measurements strong sources are necessary due to the smallness of scattering cross-section. However all the work reported here has been done in the transmission geometry. The spectrometer is calibrated by taking Mössbauer spectrum of various absorbers e.g. natural 310 Stainless Steel(S.S), $K_4Fe(CN)_6.3H_2O$, $K_3Fe(CN)_6$, $FeSO_4.7H_2O$ and iron metal etc. Only two of these are shown in Fig.2 and Fig.5. Fig.2 shows an unsplit single line Mössbauer spectrum with a paramagnetic natural 310 S.S. absorber of thickness 0.001". The theoretical value of the line width (FWHM) is 0.2 mm/sec which is twice the natural linewidth[49]. In our case it is 0.48 mm/sec which is quite satisfactory in view of the thickness of the absorber[50]. The value of isomer shift 0.34 mm/sec agrees with the reported value[51]. Fig.5 shows the Zeeman split six fingured pattern for a ferromagnetic

iron metal. The line width of the internal two lines is 0.3 mm/sec but the other lines get broadened due to the instrumental vibrations. The intensity ratios of these lines are 3:2:1 and the I.S. = 0.32 mm/sec, Q.S. = 0.08 mm/sec and internal magnetic field (H) = 330 Koe, which are in good agreement with those reported in the literature[37].

It was experienced that few sections of the spectrometer require occassional checking, more particularly the resolution of the NaI(Tl) crystal and the mercury switches. The crystal starts giving poor resolution with time due to separation of Iodine. For such a happening the crystal is remounted and original energy resolution (45%) is attained. Mercury was also purified occasionally since it gets oxidised with use.

2. PREPARATION OF SUPER COMPLEXES AND GROWTH OF SINGLE CRYSTALS

(i) Super Complexes

When cyanides of certain metals, e.g. Fe, Co, Mn, Cr are redissolved by the addition of excess of alkali cyanide solution, complex ions $[(M(CN)_6]^{4-}$ or $[M(CN)_6]^{3-}$ are formed. The alkali and alkaline earth salts of these complexes are fairly soluble in water and crystalizes well. The ferrocyanides, for example, $K_4Fe(CN)_6$ are pale yellow in colour and the ferricyanides e.g. $K_3Fe(CN)_6$

are deeper in colour and are made by oxidation of the $[M(CN)_6]^{4-}$ salts. When solutions of these complex cyanides are added to solutions of salts of 3d transition metals insoluble compounds are precipitated in many cases. Prussian blue[52], $K[Fe^{III}Fe^{II}(CN)_6]$, which is the most common compound of this class precipitates by the addition of potassium ferrocyanide to ferric salt solutions. These compounds are characterized by their stablities toward acids by the fact that they commonly contain the alkali metal ions. Such ions may be held by chemical or adsorption forces.

That these compounds are not the simple salts[53] can be understood by the reaction of the brown copper ferrocyanide, $Cu_2Fe(CN)_6.nH_2O$ (n probably 7 or 10) formed from a cupric salt and $K_4Fe(CN)_6$ such as:

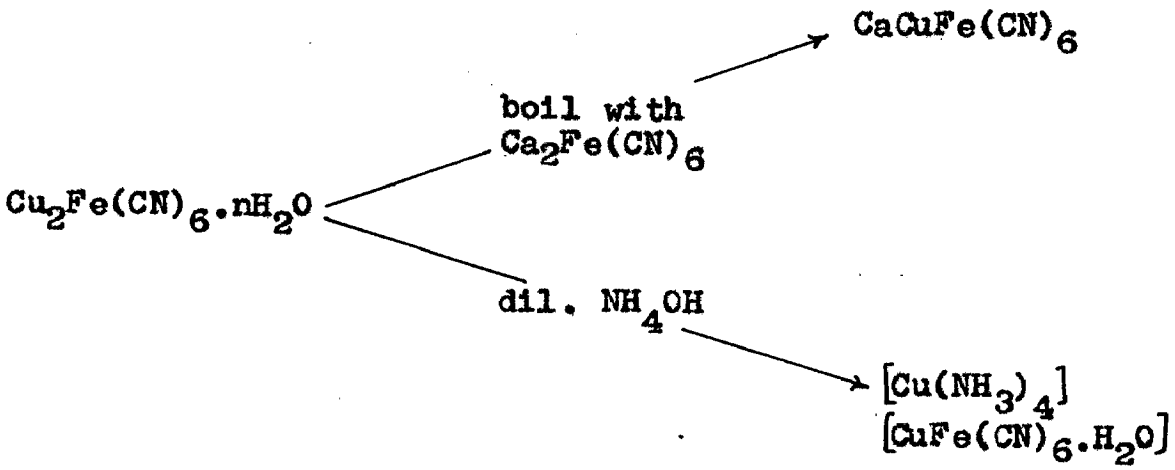

This suggest that the brown copper compound is a salt of a $CuFe(CN)_6^{2-}$ amion, viz. $Cu[CuFe(CN)_6]$. It is assumed that in these compounds the cyanide group can coordinate through the nitrogen as well as through the carbon, each

$[Fe(CN)_6]$ group can then be surrounded by the six metal ions and each metal ion by six $[Fe(CN)_6]$ groups. Thus this is a super complex as demanded by the Keggin structure[54].

The complexes under the present study are prepared by the method suggested by Prout et al[55]. A 20.8 cc of 0.5M solution of $K_4Fe^{II}(CN)_6.3H_2O$(A.R.) or $K_3Fe^{III}(CN)_6$ (A.R.) is added to 50 cc of 0.3M solution of salts of 3d transition elements viz. Cr, Mn, Fe, Co, Ni, Cu and Zn (A.R.) at room temperature over a period of 30 min. The complexes are precipitated with typical reactions such as:

$$K_4Fe^{II}(CN)_6 + Ni(NO_3)_2 \longrightarrow K_2[NiFe^{II}(CN)_6] + 2KNO_3$$

$$K_3Fe^{III}(CN)_6 + Ni(NO_3)_2 \longrightarrow K[NiFe^{III}(CN)_6] + 2KNO_3$$

The possible complexes which can be formed from the above reactions are $K_2[RFe^{II}(CN)_6]$; $R[RFe^{II}(CN)_6]$ and $K[RFe^{III}(CN)_6]$; $R_3[Fe^{III}(CN)_6]_2$, where R is a divalent 3d transition element. This suggests that the metal ion (R) replaces the alkali metal ion either partially or completely.

The slurry of these complexes is centrifuged, washed with water several times, and dried in vacuum. It is then crushed to fine powder (300 mesh) and a

50 mg/cm^2 thick layer of the complex under study is sandwiched between two perspex sheets of 1/16" thickness.

(ii) Single Crystals

The single crystals are grown from solution. Growth of single crystals demands the purity of substances, the cleaness of the apparatus used and the undisturbed slow process of evaporation. Ferrous ammonium sulphate hexahydrate and ferrous sulphate heptahydrate of guaranteed quality (G.R.) purchased from Sarabhai Mercks Limited are employed. According to the specifications, the impurities do not exceed 0.5%. The glass-ware used is cleaned by treating it with H_2CrO_4 for 48 hours. Saturated solutions of $Fe(NH_4SO_4)_2.6H_2O$ and $FeSO_4.7H_2O$ prepared at 5^o above the room temperature are allowed to evaporate from flat bottomed dishes. These are placed in an air conditioned room. A few drops of conc. H_2SO_4 are also added in the solution of $FeSO_4.7H_2O$ so as to avoid the oxidation of Fe^{2+} to Fe^{3+}. Growth of the crystals is quite slow because the concentration of the solution is only slightly more than the saturation concentration at room temperature. The grown crystals are redissolved and recrystallised for a second or even third time. The crystals selected are next tested under a polarising microscope so as to reject any twined or defective crystals. These are then coated

with liquid paraffin so as to avoid oxidation by the atmosphere.

3. CRYSTAL AXES DETERMINATION AND CUTTING IN A PARTICULAR DIRECTION

As shown in section 1, chapter IV the intensities of the two lines of a quadrupole split spectra of a single crystal absorber, depend upon the angle which the γ-rays make with the crystal axes. Firstly we describe the determination of the crystal axes for $Fe(NH_4SO_4)_2.6H_2O$ and $FeSO_4.7H_2O$ single crystals separately and then the method of cutting them in a particular direction.

(i) $Fe(NH_4SO_4)_2.6H_2O$ crystal

It is a monoclinic crystal, space group $P_{2_1/a}$, with unit cell dimensions: a = 9.28, b=12.58, c=6.22 Å and $\beta = 106^{\circ}50' 79$. The plane of symmetry of a monoclinic system is the ac plane and having identified it from the crystal habit, the $\vec{b}$-axis, which is perpendicular to the former plane, is determined. Furthermore we identified the horizontal zone[56] which is perpendicular to the $\vec{c}$-axis. It is further confirmed by measuring the angle β which tallied with the reported value. Now the remaining axis $\vec{a}$, is chosen perpendicular to $\vec{b}$ and $\vec{c}$-axis.

(ii) $FeSO_4.7H_2O$ crystal

It is also monoclinic, space group $P_{2_1/c}$, with unit cell dimensions: a=14.072, b=6.503, c=11.041 Å and $\beta = 105^{\circ}\ 34' 80$. Its (100) plane is most developed* (m plane, Fig.15) and the angle between (001) face and the edge (110) is $75^{\circ}44$ whereas between (001) and (110) faces

*The data given here is for Melanterite[57], a mineral of $FeSO_4.7H_2O$.

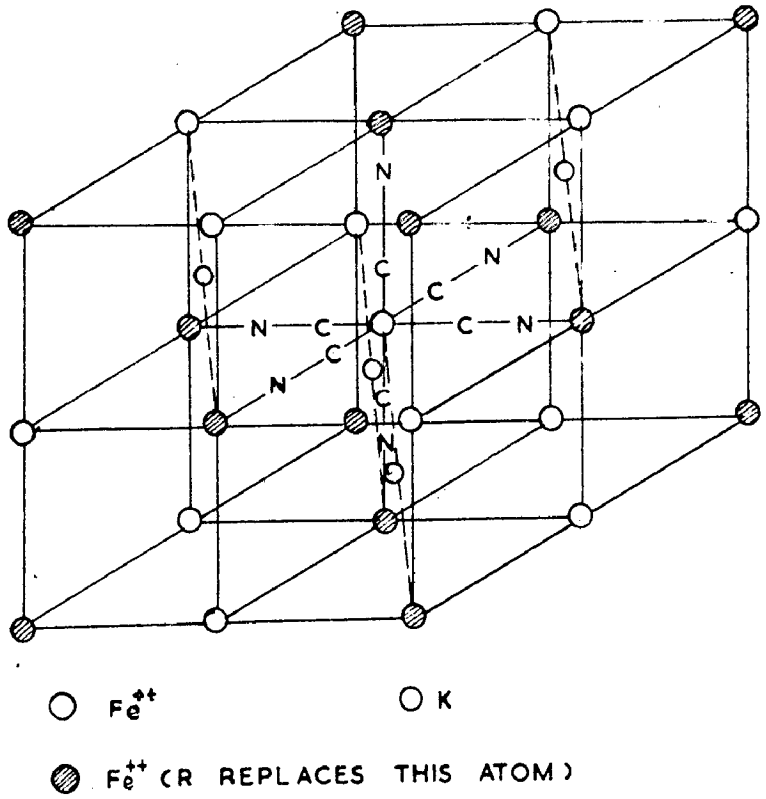

FIG.16. STRUCTURE OF POTASSIUM FERROUS FERROCYANIDE.

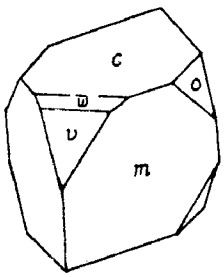

FIG.15. MONOCL[illegible] MELANTERITE, ARTIFICIAL.

is $80^{\circ}40.5'^{57}$. Crystal was mounted on a Goniometer and the ac plane or the $\vec{b}$-axis, located with the help of the above angles. The direction of $\vec{b}$-axis was further checked with cross polarizers. That the cleavages (001) and (110) are the perfect and distinct respectively and the fact that axial plane is parallel to (010) plane, enabled the identification of $\vec{b}$-axis as the Y-vibration direction. Polarized light was transmitted perpendicular to the axial plane and extinction was observed at 61° w.r. to the $\vec{c}$-axis. This agreed with the value reported in literature[56]. Thus the $\vec{b}$ and $\vec{c}$-axis were identified.

For cutting the crystal in a particular desired orientation, it was mounted on a Goniometer Head with the requirement that the cut face (which is perpendicular to the direction of γ-rays) subtended an angle of 45° with the axes of the collimeter and telescope (kept $\perp$ to each other) of an optical spectrometer. The crystal face was ground by 500 mesh emery paper and MgO powder, till a sharp image of the slit of the collimator is seen in the telescope. This ensured the planeness and verticality of the face towards the light. The other face was ground down to the thinnest possible thickness as permitted by the fragility of the sample. Final checking of the thickness ($\sim$ 0.4 mm) of the sample and the parallelism of its two faces was done on the microscope.

C H A P T E R III

FERRO- AND FERRICYANIDE SUPER COMPLEXES STUDIES*

1. INTRODUCTION

If the alkali metal ions of a ferro- and ferricyanide complex, $K_4Fe^{II}(CN)_6$ or $K_3Fe^{III}(CN)_6$ are replaced, partially or completely by the transition metal ions, new complexes are formed which have different properties. These complexes, called super complexes, form a different class. It has been shown that the cyanide group can coordinate through nitrogen as well as through carbon. Each $[Fe(CN)_6]$ group can then be surrounded by six metal ions and each metal ion by six $[Fe(CN)_6]$ groups. X-ray structural analysis of Prussian blue $K[Fe^{III}Fe^{II}(CN)_6]$, an important member of the class of the supercomplexes, had been carried by Keggin and Miles[54]. It is inferred that the complex has a face centred cubic structure, Fig.16 and forms a 3-dimensional chain Fe-C-N-Fe with half the iron atoms forming covalent and the other half ionic bonds. In this chapter we shall discuss the hyperfine structure studies of these complexes with a view to investigate the bonding and charge transfer mechanism in them.

The isomer shift, I.S., describes the energy difference for the same energy nuclear transition in the

* Part of this work is included in a paper published in J.Chem.Phys. 46, 1466 (1967).

atomic nuclei which have different s electron densities at the nuclear site e.g. at Fe^{57} nuclei in the source and absorber and is given by[26],

$$I.S. \propto S(Z) \frac{\delta R}{R} \left[|\psi(0)|^2_{Absorber} - |\psi(0)|^2_{source} \right]$$

in which S(Z) is the relativity parameter, R, is the radius of equivalent charge distribution and $|\psi(0)|^2$ is the s electron wavefunction at the iron nucleus. The second factor in the latter quantity, called the atomic or chemical parameter, is effected both by the valence state of the atom and the nature of bonding. The change in the valence state of the atom such as in Fe^{2+} and Fe^{3+}, produces a change in the s electron density at the nuclear site and shifts the nuclear levels through the altered Coulombic interaction. Thus Fe^{2+} and Fe^{3+} have different I.S. and can be distinguished on this basis whereas these cannot be distinguished by x-ray analysis.

Any ligand field asymmetry, lower than cubic, around the iron nucleus will manifest itself in the quadrupole split two line spectra. The sign of the nuclear quadrupole coupling constant e^2qQ can be inferred from the ground state orbital wavefunction, which in turn can be inferred from the magnitude of observed quadrupole splitting. However, for a more convincing assignment, one is to take recourse either to

the standard techniques (described in chapter IV) or compare with the values for a compound for which the ground state had been assigned.

Some work exists in the literature on the ferro- and ferricyanide complexes. Danon[58] and Kerler et al[59] have reported the Mössbauer investigations of ferro- and ferricyanide complexes by replacing the (CN^-) group by Co, H_2O, NO_2, NH_3, SO_3 and NO. They concluded that the s electron density increases with increasing electronegativity which means increasing tendency of ligands to withdraw 3d electrons from the neighbourhood of the iron nucleus. Matas and Zemcik[60] studied the Mössbauer spectra of $M_4Fe^{II}(CN)_6$ where M is H, Li, Na, K, Rb, Cs and NH_4 and inferred that the values of both the line shifts and linewidths depend on the electronegativity of the cations.

Duncan and Wigley[61] studied the electronic structure of iron atoms in complex iron cyanides prepared by replacing the cations by Fe^{2+} and Fe^{3+} and concluded that the cation is invariably spin free and the anion spin paired. Kerler[59] replaced potassium in $K_4Fe^{II}(CN)_6$ and $K_3Fe^{III}(CN)_6$ by Fe^{2+}, Fe^{3+}, Cu^{2+} and Ag^+ and found that in ferricyanide supercomplexes the quadrupole splitting is double its value in $K_3Fe^{III}(CN)_6$ when extrapolated to -273^oC.

A systematic investigation was undertaken of

Mössbauer spectra of potassium ferro-and ferricyanide complexes formed by replacing the cation by 3d transition elements, Cr, Mn, Fe, Ni, Co, Cu and Zn, with the expectation that such a study will provide unequivocal evidence for the change of coordination number of Fe atom. The value of I.S. will provide a sensitive test for the validity of the metal-metal charge transfer transition as advanced by Robin[52] in the case of Prussian blue.

2. EXPERIMENTAL RESULTS AND DISCUSSION

The method of preparation of the supercomplexes has been described in chapter II. These were used in the polycrystalline powder form and a thin uniform layer (~ 50 mg/cm^2) sandwiched between two perspex sheets, was placed midway between the Co^{57}(Cu) source of 1 mC initial activity and the NaI(Tl) detector. The experiment is performed at room temperature (300°K) and the results are listed in tables VI and VII for ferro- and ferricyanide supercomplexes respectively. Two typical spectra for these super complexes are shown in Fig.17 and Fig.18 respectively.

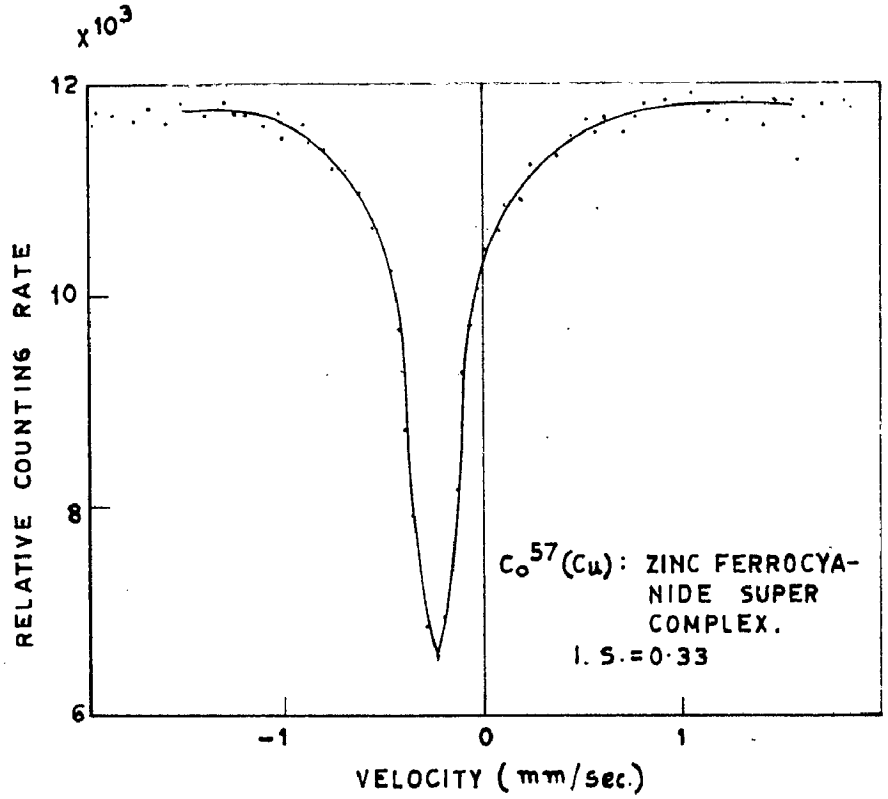

FIG. 17. TYPICAL MÖSSBOUER ABSORPTION SPECTRA FOR ZINC FERROCYANIDE SUPERCOMPLEX ABSORBER.

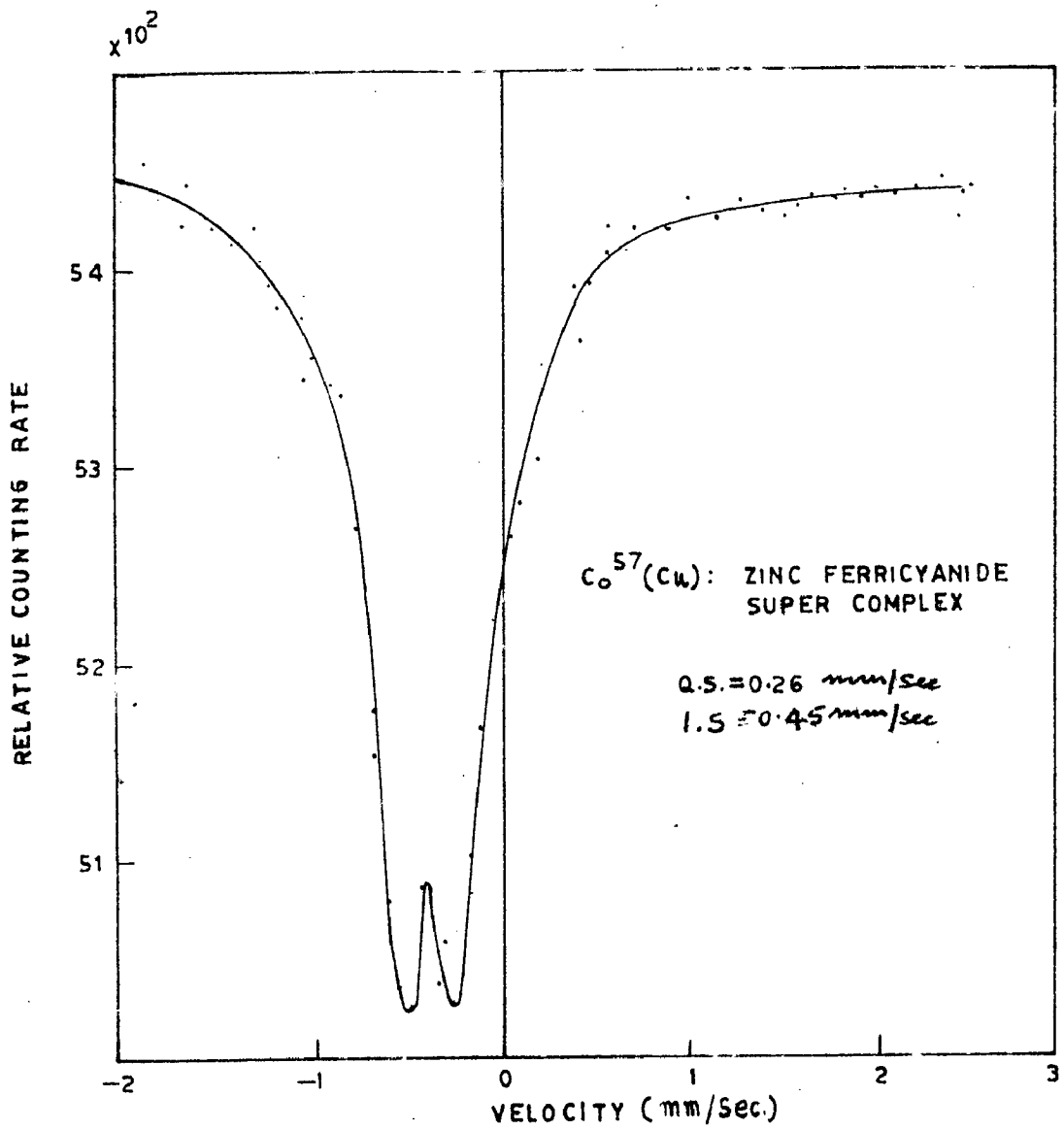

FIG. 18. TYPICAL MÖSSBAUER ABSORPTION SPECTRA FOR ZINC FERRICYANIDE SUPERCOMPLEX ABSORBER.

TABLE VI

Ferrocyanide Super Complexes

Temperature=300°K

Complex	Isomer shift (mm/sec)
1. Potassium ferrocyanide	- 0.25 ± 0.02
2. Chromium ferrocyanide	- 0.32 ± 0.02
3. Manganese ferrocyanide	- 0.34 ± 0.02
4. Iron ferrocyanide	- 0.32 ± 0.02
5. Cobalt ferrocyanide	-0.33 ± 0.02
6. Nickel ferrocyanide	- 0.34 ± 0.02
7. Copper ferrocyanide	- 0.32 ± 0.02
8. Zinc ferrocyanide	- 0.33 ± 0.02

TABLE VII

Ferricyanide Super Complexes

Temperature = 300°K

Complex	Isomer shift (mm/sec)	Quadrupole splitting (mm/sec)
1. Potassium ferricyanide	- 0.33 ± 0.02	0.26 ± 0.02
2. Manganese ferricyanide	- 0.43 ± 0.02	0.24 ± 0.02
3. Cobalt ferricyanide	- 0.43 ± 0.02	0.45 ± 0.02
4. Nickel ferricyanide	- 0.45 ± 0.02	0.46 ± 0.02
5. Copper ferricyanide	- 0.45 ± 0.02	0.43 ± 0.02
6. Zinc ferricyanide	- 0.45 ± 0.02	0.25 ± 0.02

$K_4Fe^{II}(CN)_6$ is a spin-paired, diamagnetic complex with an octahedral configuration around Fe^{2+}. On the valence bond model the Fe^{2+} ion has the hybridization d^2sp^3. On the basis of observed magnetic moment it has been classified as an essentially covalent complex[62] with the following assigned structure:

$$(CN)_5Fe^{(-3)} = C = \ddot{N}:^{(-1)}$$

The CN^- groups are linked to the central atom by σ bonds. Furthermore each bond has a partial π component which removes charge from the central atom in accordance with

the Pauling electronegativity principle[62]. Magnetic moment data show that $K_3Fe^{III}(CN)_6$ is also a covalent complex and thus both these are in a strong field of their ligands. In the presence of ligands, the five d orbitals split into two degenerate groups, the doubly degenerate $3d_{x^2-y^2}$ and $3d_{z^2}$ (called e_g) group lie higher than the triply degenerate $3d_{xy}$, $3d_{yz}$, and $3d_{xz}$ (called t_{2g}) group in octahedral symmetry. The strong field configuration demands all the 3d electrons to lie in t_{2g} orbitals resulting in the spin-paired complexes in both the cases, Fig.19. Thus in $K_4Fe^{II}(CN)_6$ all the $3d^6$ electrons of Fe^{2+} are spin-paired and give rise to spherically symmetric electric field making the complex diamagnetic. Whereas in $K_3Fe^{III}(CN)_6$ one 3d electron is spin free (Fig.19) which gives rise to paramagnetism of the complex. The vacancy in the t_{2g} levels gives rise to the electric field gradient responsible for the observed quadrupole spectra.

Let us now consider the super complexes. Keggin and Miles inferred that these substances form cubic crystals in which iron atoms lie at the points of a simple cubic lattice, each being connected with its six neighbours of CN groups extending along the cube edges (Fig.16). The potassium ions and water molecules lie in the cubes outlined in this way. Magnetic susceptibility measurements

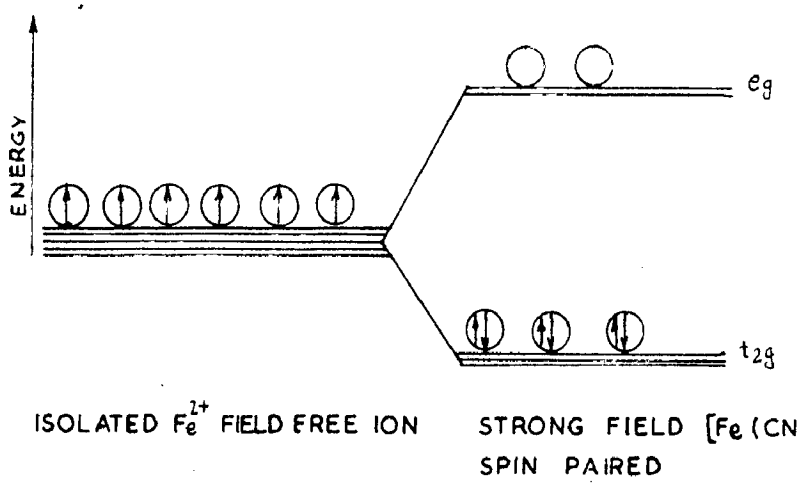

FIG.19. ENERGY LEVEL DIAGRAGM OF Fe^{2+} ION IN STRONG FIELD OF ITS LEGANDS. THE e_g LEVELS ARE 'DOUBLY DEGENERATE AND THE t_{2g} LEVELS ARE TRIPLY DEGENERATE.

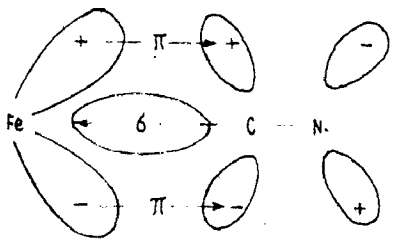

FIG.20 DIAGRAMMATIC REPRESENTATION OF BONDING RELATIONSHIP BETWEEN IRON AND A LIGAND WITH A Δ ORBITAL.

show that half of the iron atoms, presumably those bonded to the carbon atoms of the six adjacent cyanide groups, form covalent bonds; whereas the other iron atoms form ionic bonds. However the valence state of the iron atoms cannot be inferred unequivocally from these measurements. The complexes, under study here, have the structure identical to that of $K_2[FeFe(CN)_6]$ with atom-for-atom substitution of R (Cr, Mn, Fe, Co, Ni, Cu and Zn) for Fe^{2+}. The value of the I.S. in these complexes, table VI and VII, are of the same order of magnitude as in the case of covalently bonded Fe^{2+} complexes. This suggests that the substituted R atoms replace only those Fe^{2+} atoms which a re bonded ionically with N atoms, Fig.16.

The cyano groups in $[Fe(CN)_6]^{4-}$ are linked to the central iron atom by σ bonds and each bond has a π component which prevents the build-up of a high negative charge on iron (back donation). The bond relationships are depicted in Fig.20. According to Pauling's principle of electroneutrality the central atom can never have charge greater than +1 or -1, and in accordance π bond removes charge from the central atom. The ionicity of an ion becomes weaker with the decrease in coordination number. The constancy of the values of the I.S. in these ferro- and ferricyanide super complexes, Tables VI and VII, makes it possible to state that the coordination number of the central Fe^{2+} atom remains six in all these complexes.

The argument is based on the fact that there are three π bonds present in the octahedral complexes such as: $K_4Fe^{II}(CN)_6$ and $K_3Fe^{III}(CN)_6$. If the coordination number becomes four now in the super complexes[63] then the available CN^- ligands around Fe atom are four and the π bonds should become two with the consequence that the overall π bond component would become smaller. Thus the decrease of coordination number reduces the withdrawal of 3d electrons from the central metal atom. This increase of 3d electron density will shield the 4s electrons to a larger extent and reducing thereby the s electron density at the nucleus. This will cause the I.S. to be less negative. As our values for I.S. are more negative, the plausibility of the decrease of coordination number[63] on the formation of super complexes does not hold.

The charge transfer mechanism in these complexes can be understood with the help of the molecular orbital diagram to be expected for Fe^{2+} and Fe^{3+} ions in the carbon holes as well as the nitrogen holes. The molecular orbital diagram for $KFe^{III}Fe^{II}(CN)_6$ as given by Robin[52] is shown in Fig.21. The molecular orbitals for the cyanide ions are shown at the centre in this Fig. and the ordering of the levels being derived from the previously assigned bands of the cyanide radical. Depending upon whether the nitrogen or the carbon ends of

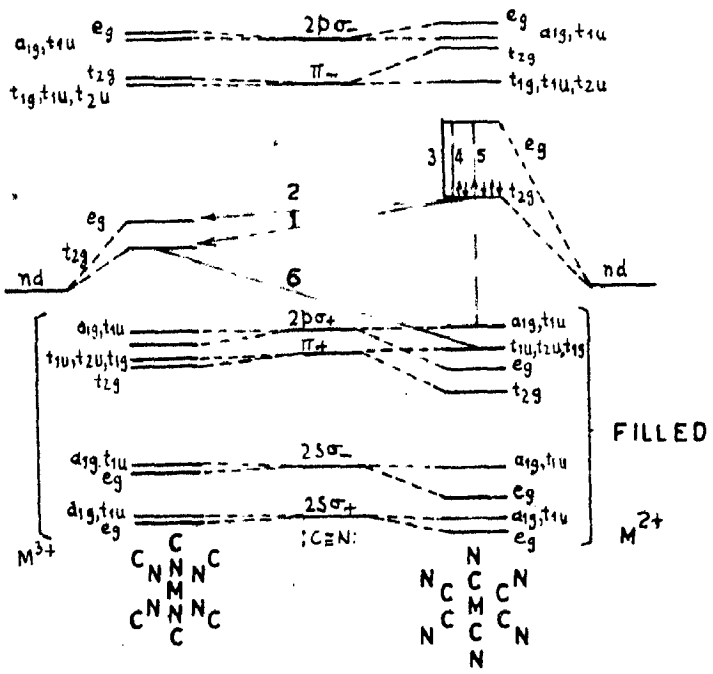

FIG. 21. A MOLECULAR ORBITAL SCHEME FOR PRUSSIAN BLUE. THE SYMMETRY LABELS ON ANY COLUMN OF LEVELS ARE APPROPRIATE ONLY TO THE MOLECULE LISTED AT THE FOOT OF THAT COLUMN

the CN^- ligands coordinate with the metal ions, metal-ligand orbital may be assumed to form, as shown on either the left or the right hand side in Fig.21. The metal ion in the carbon hole invariably has low spin, strong field configuration indicative of a large splitting of the metal ion d orbitals. Robin has attributed the colour of Prussian blue, $KFe^{III}Fe^{II}(CN)_6$ to a charge transfer transition between $[Fe^{II}(CN)_6]^{4-}$ and Fe^{3+} ions. The conclusion is based on the fact that Fe^{2+} which is in a carbon hole is in a strong field, whereas the Fe^{3+} is in a nitrogen hole and in a weak field. The strong field configuration is indicative of larger splitting then the weak field case and the charge transfer is rendered probable. Our values of I.S. for both the ferro and ferricyanide super complexes are more negative than for $K_4Fe^{II}(CN)_6$ and $K_3Fe^{III}(CN)_6$ respectively, because the 3d atoms linked to the N atom act as accepters of charge reducing thereby the 3d electron density at the central iron atom. This will make the I.S. more negative as supported by the experimental data. Furthermore from the constancy of the values of the I.S. in the case of ferro and ferrigroups of super complexes it is inferred that the different electronegativities of the substituents have no perceptible effect on the s electron density at Fe nucleus. This seems plausible in view of the Fe-R

distance of 5.1 Å.

No quadrupole splitting is expected in ferro super complexes, because octahedral Fe^{2+} complex is in a spin paired, strong field configuration which makes the 3d electron charge distribution spherosymmetrical. On the other hand, octahedral Fe^{3+} super complexes have an unpaired spin in the strong field configuration. Thus we get a two line Mössbauer spectrum for this case. The experimental observations show that the quardrupole aplitting is nearly double in all ferri super complexes (with the exception of Mn and Zn super complexes) as compared to $K_3Fe^{III}(CN)_6$. As mentioned earlier in octahedral symmetry 3d orbitals split into two degenerate groups t_{2g} ($m_l = -2, \pm 1$) and e_g ($m_l = 0,2$) levels. The e_g orbitals are occupied by the d^2sp^3 hybrids and the five d electrons in $K_3Fe^{III}(CN)_6$ occupy the t_{2g} orbitals. Since the half shell can be considered closed there, are two electrons (maximum number of electrons that can be accommodated in t_{2g} orbitals is six) to be distributed in the remaining $3t_{2g}$ orbitals. This may be considered as a perturbation over the octahedral crystal field and thus cause the partial removal of the degeneracy of the t_{2g} orbitals into $3d_{xy}$ and $3d_{yz}$, $3d_{xz}$. As $\frac{\partial^2 V}{\partial z^2}$ is proportional to ($m_l^2 - 2$) including the sign, the field gradient will be proportional to +1 if $3d_{xy}$ lies lower

and -2 if $3d_{xy}$ lies higher than the $3d_{yz}$, $3d_{xz}$ doublet. Thus the value of quadrupole splitting depends on the relative energies of the $3d_{xy}$ and $3d_{yz}$, $3d_{xz}$ orbitals. Hence the value of quadrupole splitting in super complexes of ferricyanide, which is two times the Q.S. for $K_3Fe^{III}(CN)_6$ suggest that in $K_3Fe^{III}(CN)_6$ the $3d_{xy}$ level lies lower and in super complexes (Cr, Fe, Ni, Co and Cu) it lies higher than the other two degenerate orbitals. In the case of Mn^{2+} and Zn^{2+}, the number of 3d electrons is 5 and 10 respectively, and as the half-filled shell viz. Mn^{2+} can be considered to be closed viz. Zn^{2+}; these two cases do not cause any perturbation so that ΔE_q is comparable to that of $K_3Fe^{III}(CN)_6$. This explains the observed quadrupole splitting in these two cases. It is obvious that the ground state wavefunction is the singlet $3d_{xy}$ in the case of Mn^{2+} and Zn^{2+} super complexes whereas it is the doublet $3d_{yz}$ and $3d_{xz}$ in the case of the rest. On this basis it may be stated that the sign of quadrupole coupling constant e^2qQ is positive in the case of Fe, Ni, Co and Cu whereas negative for Zn and Mn super complexes.

C H A P T E R IV

NUCLEAR ELECTRIC FIELD GRADIENT DETERMINATION IN SINGLE CRYSTALS OF $Fe(NH_4SO_4)_2.6H_2O$ AND $FeSO_4.7H_2O$*

1. INTRODUCTION

The Hamiltonian of the interaction of the quadrupole moment of the nucleus with the field gradient at its position due to surrounding charges is given by the scaler tensor product[65]

$$\mathcal{H}_Q = \bar{Q} \cdot \bar{\nabla} E \qquad (26)$$

where $\bar{Q}$ is the tensor defining the quadrupole charge distribution in the nucleus, and the field gradient at the nucleus is defined by the tensor $(\bar{\nabla} E')$ having 9 components $-V_{ij}$ in cartesian coordinates, where

$$V_{ij} = \frac{\partial^2 V}{\partial x_i \partial x_j} \qquad (x_i, x_j = x, y, z)$$

and V is the electrostatic potential at the nucleus. This is caused by both the aspherical charge distribution of the ion and the charges at surrounding lattice-sites. As the electric field gradient at the nucleus

---

* Part of this work is encluded in a paper communicated to Phys. Rev.

will be produced entirely by the charges external to it, it satisfies Laplace's equation viz. $V_{xx}+V_{yy}+V_{zz}=0$. The tensor is traceless, symmetric having five irreducible components. However this symmetric tensor can be diagonalized by transforming to an orthogonal set of principal axes x', y', z', and the resulting irreducible components are:

$$
\begin{aligned}
(\nabla E)_0 &= \tfrac{1}{2} V_{z'z'} = \tfrac{1}{2} eq \\
(\nabla E)_{\pm 1} &= 0 \\
(\nabla E)_{\pm 2} &= \frac{1}{2\sqrt{6}} \left(V_{x'x'} - V_{y'y'} \right) = \frac{1}{2\sqrt{6}} \eta q
\end{aligned}
\qquad (27)
$$

e^2qQ is termed as quadrupole coupling constant for the nucleus in a particular environment under consideration and its sign has important structural implications. The three independent components in Eq.27 are related by Laplace Eq. and so there are only two independent components left to specify the field gradient tensor completely. These are:

$$eq = V_{z'z'}$$

and

$$\eta = \frac{V_{x'x'} - V_{y'y'}}{V_{z'z'}} \quad \text{(called the asymmetry parameter)}$$

with $|V_{z'z'}| \geq |V_{x'x'}| \geq |V_{y'y'}|$ for which $0 \leq \eta \leq 1$. [66]

Hence the field gradient tensor can be specified completely in a laboratory system of coordinates if the Eulerian angles (α, β, γ) describing the relative orientations of principal axes system and laboratory system are known[66] . The field gradient tensor can thus be specified completely by five quantities eq, η, α, β and γ . In this chapter we shall determine these quantities in the single crystals of $Fe(NH_4SO_4)_2 .6H_2O$ and $FeSO_4.7H_2O$. Furthermore quadrupole coupling constant, e^2qQ, will also be determined from Mossbauer studies.

The orientation of EFG axes and the sign of nuclear quadrupole coupling constant has been determined from the Zeeman effect studies in nuclear quadrupole resonance and molecular beam spectroscopy[65] for the nuclei having ground state quadrupole moment. Alff and Wertheim[67] determined the sign for Yttrium iron garnet single crystals by cutting them normal to (110) and magnetized along (100) direction and studying the Mössbauer spectrum absorption dips. Wertheim[68] also determined the sign and magnitude of e^2qQ in single crystals of FeF_2 by using single crystals cut in directions parallel and perpendicular to the ĉ-axis. Sign of quadrupole coupling constant in sodium nitroprusside was determined by Danon[58] from the single crystal spectra by analyzing the line

intensities as a function of orientation. For crystals having mixed quadrupole and magnetic interaction, the sign of e^2qQ was determined by analyzing the line intensities as a function of orientation. The line intensities for such crystals are[69]

$$\begin{aligned} I_1 &= \frac{1}{4\pi}\frac{1}{2}(1+\cos^2\theta) = I_6 \\ I_2 &= \frac{1}{4\pi}\frac{2}{3}\sin^2\theta = I_5 \\ I_3 &= \frac{1}{4\pi}\frac{1}{3}\frac{1}{2}(1+\cos^2\theta) = I_4 \end{aligned} \qquad (28)$$

where θ is the angle the γ radiation makes with the spin axis. Johnson[69] determined these parameters for $FeCl_2.2H_2O$. Ono and Ito [70] determined the sign of the quadrupole coupling constant and hence the ground state wavefunction for several ferrous salts having magnetic transitions above 4^oK and in the presence of sufficiently large internal field. In addition, the sign of e^2qQ has been determined from absorption spectra obtained with a potarized source[71] and from the anisotropy of lattice vibrations[32] with some knowledge of the crystal or molecular structure[72]. Another very useful and fairly general technique using a magnetic perturbation was proposed[73] and applied to determine the sign of e^2qQ in ferrocene[74]. The last method was applied to determine the sign of e^2qQ in case of ferrous compounds[75]

and has the advantage of its applicability to powdered samples. It makes use of the fact that in the presence of sufficiently large magnetic field $\bar{H}_{ext}$ 30KOe, a simple two-line quadrupole split absorption pattern of iron atom in either the paramagnetic or diamagnetic state will split into a triplet and a doublet, the doublet lying higher in energy for a positive e^2qQ. However it is difficult to determine the sign of coupling for the compounds having large η e.g. $Fe(NH_4SO_4)_2.6H_2O$. Another useful method was first suggested and applied by Zory[76] and is based on the fact that the emission and absorption probabilities of both the hyperfine components ($\pm$ 3/2 $\longrightarrow$ $\pm$ 1/2 and $\pm$ 1/2 $\longrightarrow$ $\pm$ 1/2) are different in respect to the direction of the EFG axes[77,78]. Since the EFG depends on the electronic state of the atom, from measurements of the spectra of single crystals, one can infer both the ground state orbital wavefunction and the sign of the quadrupole coupling constant. Making use of this method we shall determine all the five parameters of the EFG tensor for the first excited state of Fe^{57} in single crystals of $Fe(NH_4SO_4)_2.6H_2O$ and $FeSO_4.7H_2O$.

2. CRYSTAL STRUCTURE

(i) Ferrous Ammonium Sulphate Hexahydrate $Fe(NH_4SO_4)_2.6H_2O$

It is a monoclinic crystal, space group $P_{21/a}$,

with unit cell dimensions a = 9.28, b = 12.58, c = 6.22 Å and $\beta = 106^{\circ}50'$ [79]. The unit cell contains two equivalent Fe^{++} ions at (0,0,0) and (1/2,1/2,0), each ion surrounded by a distorted octahedron constructed from six water molecules. All the atoms except Fe^{++} in the typical $Fe(NH_4SO_4)_2.6H_2O$ have been placed in general positions

$$e \quad : \quad \pm \ (x, y, z; \ x + 1/2, \ 1/2 - y, \ z)$$

These octahedra are related to each other through a rotation of 180° about b axis, disregarding the translation operations, since it is only the orientation of sites relative to the crystal axes which are important in such studies. The projection diagram along (010) for $Mg(NH_4SO_4)_2.6H_2O$ which is isomorphous to $Fe(NH_4SO_4)_2.6H_2O$ is shown in Fig.22 and the bond length and bond angles for the isomorphous $Zn(NH_4SO_4)_2.6H_2O$ are tabulated in Table VIII.

TABLE VIII

Bond lengths and bond angles of coordination octahedron around Zn

Zn--OW(7) = 2.129 (0.012) Å

Zn--OW(8) = 2.117 (0.012) Å

Zn--OW(9) = 2.075 (0.012) Å

OW(9)-Zn-OW(7) = 89.1° (0.04)

OW(8)-Zn-OW(7) = 90.6° (0.04)

OW(8)-Zn-OW(9) = 89.2° (0.04)

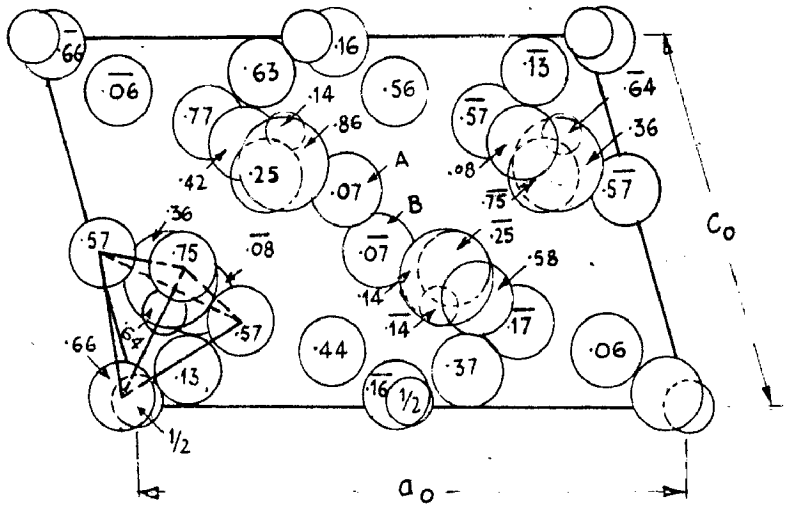

FIG.22. PROJECTION OF THE MONOCLINIC STRUCTURE OF $Mg(NH_4SO_4)_2 \cdot 6H_2O$ ON ITS b-FACE. OXYGEN ATOMS OF THE SULFATE IONS NEAR THE ORIGIN ARE CONNECTED BY LINES. THE NH_4^+ IONS ARE SHOWN AS THE LARGEST CIRCLES, THE MAGNESIUM ATOMS BY CIRCLES SLIGHTLY LARGER THAN THE (SMALLEST) SULFUR CIRCLES. WATER MOLECULES ARE THE HEAVILY RINGED CIRCLES.

(ii) Ferrous sulphat Heptahydrate $FeSO_4.7H_2O$

The crystal structure of $FeSO_4.7H_2O$ has been investigated by Bauer[80] through x-ray analysis. The projection diagram along (010) is given in Fig.23. It crystallises in monoclinic crystals, space group $P2_{1/c}$, with unit cell dimensions a = 14.072 (10), b = 6.503 (7), c = 11.041 (10)Å , $\beta = 105^{\circ}\ 34'$ (5) and Z = 4. It was assumed that the iron atoms occupy the special positions (a) 000, $0\ \frac{1}{2}\ \frac{1}{2}$ and (d) $\frac{1}{2}\ \frac{1}{2}\ 0$, $\frac{1}{2}\ 0\ \frac{1}{2}$, thus forming a face centred arrangement. Positions (a) and (d) have the point symmetry $\bar{1}$, as have the other two special positions (b) and (c).

The first neighbours of Fe^{++} atoms are the water molecules forming the slightly distorted octahedron. The interatomic distances and bond angles between the Fe^{++} sites and water molecules are given in Table IX.

TABLE IX

Interatomic Distances and Bond Angles

(a) Coordination octahedron around Fe(1)

Fe(1) - OW(1) = 2.068 (5)Å

Fe(1) - OW(2) = 2.144 (5)Å

Fe(1) - OW(3) = 2.136 (5)Å

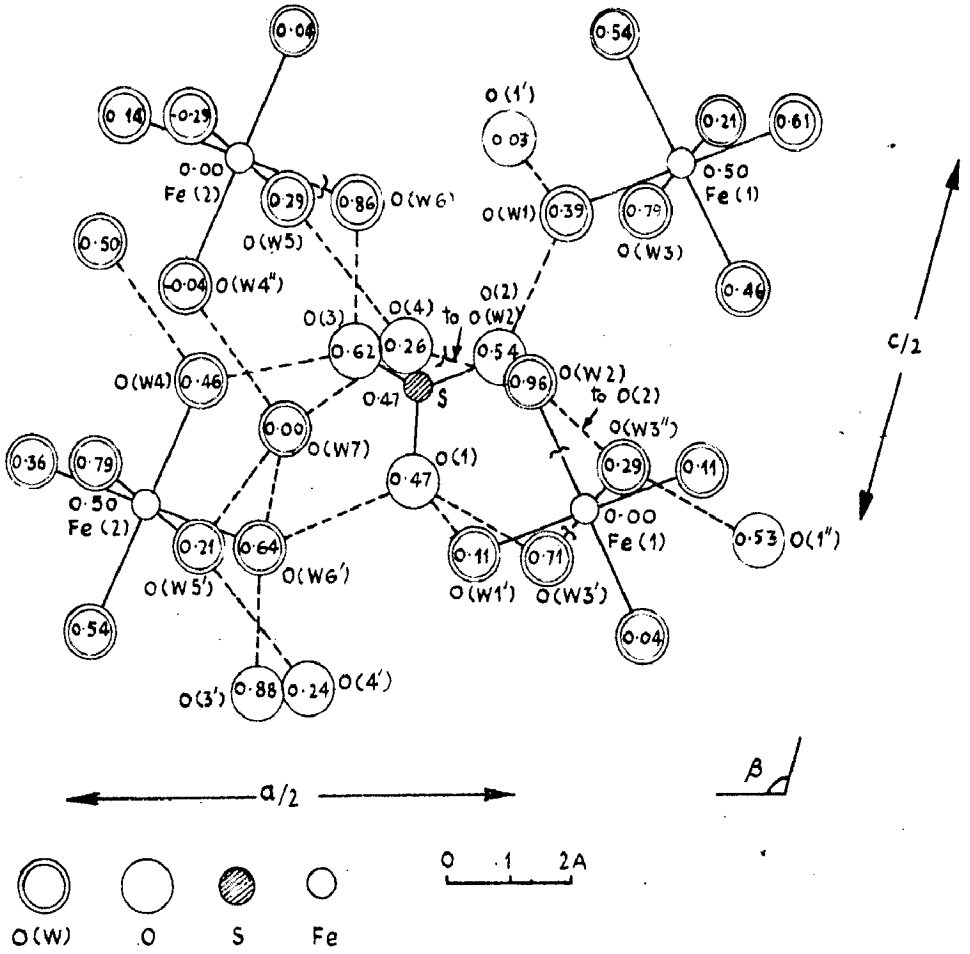

FIG. 23. PROJECTION OF THE MONOCLINIC STRUCTURE OF $FeSO_4.7H_2O$ IN (010) DIRECTION.

OW(1) - Fe(1) - OW(2) = 90.5° (0.2)
OW(1) - Fe(1) - OW(3) = 92.9° (0.2)
OW(2) - Fe(1) - OW(3) = 94.0° (0.2)

(b) Coordination Octahedron around Fe(2)

Fe(2) - OW(4) = 2.096 (5)Å
Fe(2) - OW(5) = 2.109 (5)Å
Fe(2) - OW(6) = 2.188 (5)Å

OW(4) - Fe(2) -OW(5) = 90.5°(0.2)
OW(4) - Fe(2) -OW(6) = 91.0°(0.2)
OW(5) - Fe(2) -OW(6) = 92.4°(0.2)

3. ORBITAL WAVE FUNCTIONS AND ELECTRIC FIELD GRADIENT

The spin Hamiltonian (Eq.26) can be rewritten in the principal axes system as:

$$\mathcal{H}_Q = \frac{e^2qQ}{4}\left[I_z^2 - \frac{5}{4} + (\eta/6)(I_+^2 + I_-^2)\right] \qquad (29)$$

where I_+ and I_- are the step up and step down operators. Fe^{57} has $I = \pm 1/2$ ground state which precludes a quadrupole interaction. The 14.4 keV level of this nucleus has $I = \pm 3/2$ which causes a quadrupole splitting in the presence of electric field gradient. The separation between these two peaks is given by ΔE_Q:

$$\Delta E_Q = \frac{e^2|q|Q}{2}\left[1 + \frac{\eta^2}{3}\right]^{1/2} \qquad (30)$$

In order to account for the effect of lattice, the above EFG components are expressed as

$$\frac{V_{zz}}{e} = q = (1-R)\, q_{ion} + (1-\gamma_\infty)\, q_{lat} \qquad (31)$$

and $$\frac{V_{xx}-V_{yy}}{e} = \eta q = (1-R)\,\eta_{ion}\, q_{ion} + (1-\gamma_\infty)\, q_{lat}\,\eta_{lat}$$

The subscripts ion and 'lat' stand for the charge distribution of the aspherical 3d valence electrons belonging to the ferrous ion (^5D, $3d^6$) and the neighbouring ions in the crystalline lattice respectively. (1-R) and ($1-\gamma_\infty$) are the sternheimer factors which are introduced to correct for the polarization of the ferric like (^6S, $3d^5$) core by the EFG of the ion and lattice charge distributions.

In these crystals the Fe^{++} ions are in a spin free state and are surrounded by distorted octahedra of water molecules. In low ligand fields of octahedral symmetry this will normally split into a lower energy degenerate triplet $|xy\rangle$, $|xz\rangle$, $|yz\rangle$ called t_{2g} orbitals and higher energy degenerate doublet $|x^2-y^2\rangle$ and $|3z^2-r^2\rangle$ called e_g orbitals. If the octahedra is distorted one, then a small ligand field of a symmetry lower than cubic such as axial and rhombic[81] will lift the degeneracy further as shown in Fig.24.

The EFG arises from the aspherical charge distribution of the ^5D, $3d^6$ ferrous ion over t_{2g}

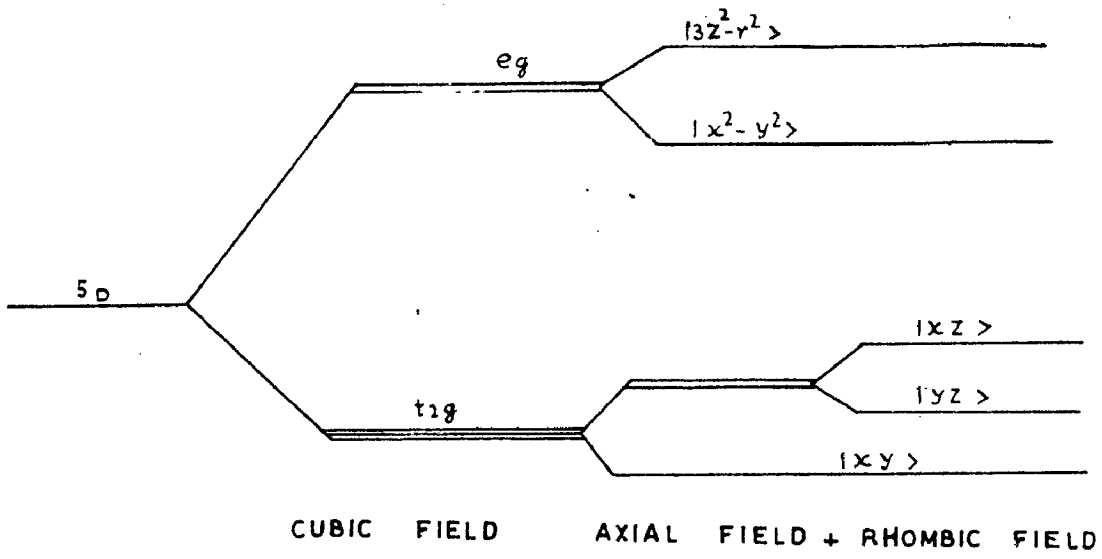

FIG. 24. ENERGY LEVEL SCHEME OF Fe^{++} ION UNDER THE ACTION OF A CRYSTALLINE FIELD ARISING FROM A DISTORTED OCTAHEDRON.

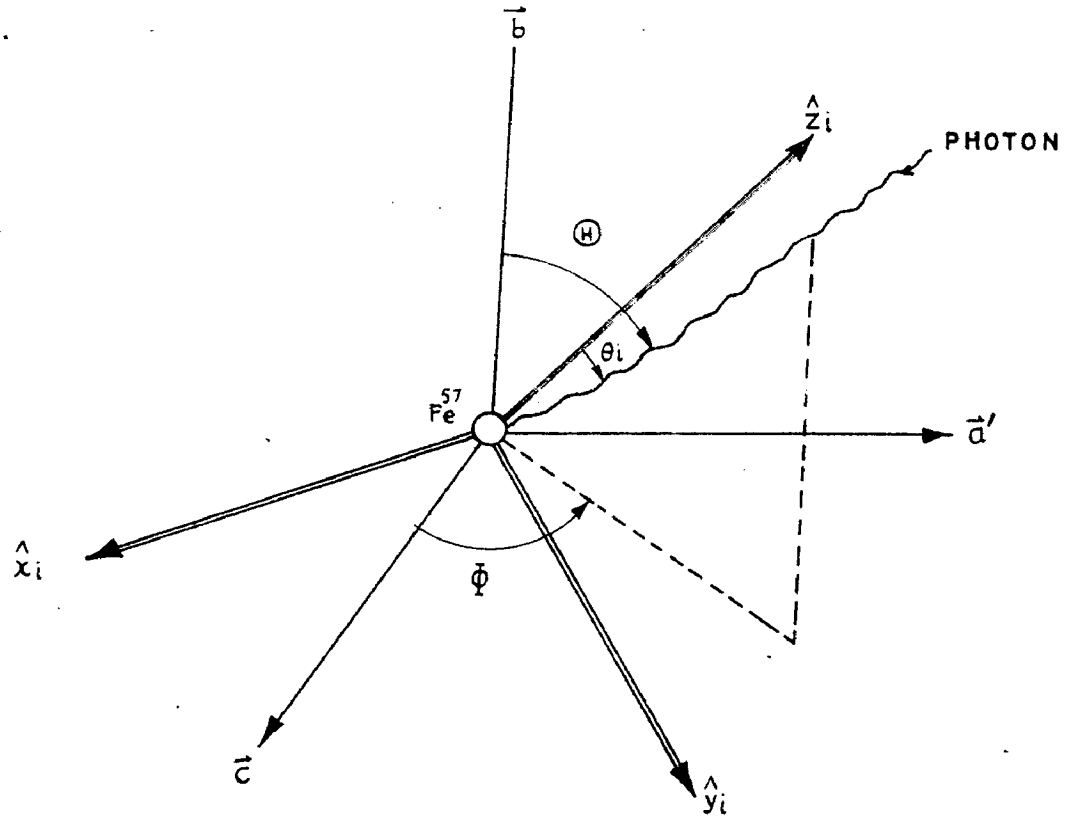

FIG. 25. SCHEMATICS OF THE ABSORPTION OF 14·4 keV-RAY BY Fe

orbitals. The field gradient parameters for e_g and t_{2g} orbitals are [82]

Orbital wavefunction	q_{ion}	η_{ion}
$\|xy\rangle$	$(4/7)\ \langle r^{-3}\rangle_{3d}$	0
$\|xz\rangle$	$-(2/7)\ \langle r^{-3}\rangle_{3d}$	3
$\|yz\rangle$	$-(2/7)\ \langle r^{-3}\rangle_{3d}$	-3
$\|3z^2 - r^2\rangle$	$-(4/7)\ \langle r^{-3}\rangle_{3d}$	0
$\|x^2 - y^2\rangle$	$(4/7)\ \langle r^{-3}\rangle_{3d}$	0

The determination of the sign of quadrupole coupling constant e^2qQ will determine whether the ground state is a singlet $|xy\rangle$ or doublet $|xz\rangle$, $|yz\rangle$

4. METHOD OF ANALYSIS

The EFG parameters are determined from the absorption peak areas of the quadrupole doublet for various orientations of the γ-ray beam with respect to the crystal axes. The absorption spectrum line areas are of particular interest because they are independent of source line shape and instrumental velocity resolution and also because they saturate less rapidly with increasing absorber thickness than do the associated heights.

The area under the n-th absorption for a single crystal absorber with one absorbing nucleus per unit cell and a monochromatic unpolarized source is[83]:

$$a_n \approx \int_0^\infty \left(1 - \exp\left[\sigma_n(E,\theta,\phi) f'(\theta,\phi)\omega\right]\right) dE \qquad (32)$$

where

$\sigma_n(E,\theta,\phi)$ ≡ energy dependent nuclear resonance absorption cross section per nucleus for transition n in the direction (θ,ϕ) relative to the field causing the splitting.

$f'(\theta,\phi)$ ≡ recoilless absorption probability whose angular dependence derives from the anisotropy in the mean square displacement of the vibrating nucleus.

ω ≡ surface density of atoms capable of resonant absorption.

Assuming $\sigma_n(E,\theta,\phi) f'(\theta,\phi)\omega << 1$ and restricting to dipolar radiation only it has been shown by Zory[76] that Eq.32 reduces to

$$a_n \sim f'(\theta,\phi)\, p_n(\theta,\phi) \qquad (33)$$

where $p_n(\theta,\phi)$ is the angular dependent absorption probability for transition n.

If instead of one absorbing nucleus per unit cell the crystal has two or more equivalent sites per unit cell* then the area ratios for transitions 3 and 1 for an Fe^{57} nucleus is given by

$$\frac{a_3}{a_1} = \frac{\sum_{i}^{sites} p_3(\theta_i, \phi_i) f'(\theta_i, \phi_i)}{\sum_{i}^{sites} p_1(\theta_i, \phi) f'(\theta_i, \phi_i)} \qquad (34)$$

where the transitions '3' and '1' refer to the transitions $\pm 3/2 \longrightarrow \pm 1/2$ and $\pm 1/2 \longrightarrow \pm 1/2$ respectively. The presence of inequivalent sites will produce the multiline spectra and such cases can also be treated with Eq. 34 with proper grouping of the lines according to their origin. Eq.34 for powder absorbers reduces to:

$$\frac{a_3}{a_1} = \frac{\int_{4\pi} p_3(\theta, \phi) f'(\theta, \phi)\, d\Omega}{\int_{4\pi} p_1(\theta, \phi) f'(\theta, \phi)\, d\Omega} \qquad (35)$$

In order to use Eq.34 let us express it in terms of nuclear EFG parameters. Fig.25 gives the experimental situation. Since both the crystals under the present investigation are monoclinic we introduce an axis $\vec{a}'$ constructed so that the axes $\vec{a}'$, $\vec{b}$ and $\vec{c}$ are mutually orthogonal. The unit vectors $(\hat{x}_1, \hat{y}_1, \hat{z}_1)$

* If the environment of the absorbing nuclei is the same but differ in orientation only, the two sites are called to be equivalent.

Locate the principal axes of EFG of i-th site, the three Euler angles ($\alpha_i, \beta_i, \gamma_i$), designating their orientations relative to ($\vec{a}', \vec{b}, \vec{c}$) being unknown. Angles θ_i, ϕ_i are the orientation angles of the incident beam relative to ($\hat{x}_i, \hat{y}_i, \hat{z}_i$). Let us introduce angles Θ, Φ the polar and azimuthal angles of the incident photon beam relative to the ($\vec{a}', \vec{b}, \vec{c}$) axes.

The expressions for relative transition probabilities p_3 and p_1 were derived by utilizing the fact that 14.4 keV γ-ray is a magnetic dipolar radiation[84] and are given by

$$p_3(\theta,\phi) = 4\left(1+\frac{\eta^2}{3}\right)^{1/2} + \left(3\cos^2\theta - 1 + \eta \sin^2\theta \cos 2\phi\right)$$
$$p_1(\theta,\phi) = 4\left(1+\frac{\eta^2}{3}\right)^{1/2} - \left(3\cos^2\theta - 1 + \eta \sin^2\theta \cos 2\phi\right) \qquad (36)$$

Expressing $\cos^2\theta_i$ and $\sin^2\theta_i \cos 2\phi_i$ in terms of the known experimental angles Θ, Φ and the unknown Euler angles relating site i to axes ($\vec{a}', \vec{b}, \vec{c}$), we express Eq.34 after inserting the values for p_3 and p_1 from Eq.36 and assuming the isotropy of $f'(\theta, \phi)$:

$$\frac{a_3}{a_1} = \frac{\sum_{sites}\left\{4\left(1+\frac{\eta^2}{3}\right)^{1/2} + (3K - 1 + \eta K')\right\}}{\sum_{sites}\left\{4\left(1+\frac{\eta^2}{3}\right)^{1/2} - (3K - 1 + \eta K')\right\}} \qquad (37)$$

where $K = \sin^2\Theta\left[\cos^2\Phi\, Z_{a'}^2 + \sin^2\Phi\, Z_c^2\right] + \cos^2\Theta\, Z_b^2$
$+ \sin^2\Theta \sin 2\Phi\, Z_{a'} Z_c + \sin 2\Theta\left[\sin\Phi\, Z_c Z_b + \cos\Phi\, Z_{a'} Z_b\right]$

$$k' = \sin^2\Theta\left[\cos\Phi\,(x_{a'}^2 - y_{a'}^2) + \sin^2\Phi\,(x_c^2 - y_c^2)\right]$$
$$+ \cos^2\Theta\,(x_b^2 - y_b^2) + \sin^2\Theta\,\sin 2\Phi\,(x_{a'}x_c - y_{a'}y_c)$$
$$+ \sin 2\Theta\left[\cos\Phi\,(x_{a'}x_b - y_{a'}y_b) + \sin\Phi\,(x_c x_b - y_c y_b)\right]$$

The symbols Xá, Yb etc. denote the direction cosines $\hat{x}.\vec{a}$, $\hat{y}.\vec{b}$ etc. These direction cosines can be expressed as a function of the same Euler angles α, β, γ [85].

In $Fe(NH_4SO_4)_2.6H_2O$ there are only two equivalent sites per unit cell and these are related to each other through a rotation of 180° about b axis. In $FeSO_4.7H_2O$ there are four such sites. These sites form two distinct sites (1 and 2) each site includes the site having the point symmetry $\bar{1}$. Eq.37 thus becomes:

$$\frac{a_3}{a_1} = \frac{\left[8(1+\eta^2/3)^{1/2} + \{3(k+\bar{k}) - 2 + \eta(k'+\bar{k}')\}\right]}{\left[8(1+\eta^2/3)^{1/2} + \{3(k+\bar{k}) - 2 + \eta(k'+\bar{k}')\}\right]} \quad (38)$$

where the quantities $(K, \bar{K}')$ and $(\bar{K}, \bar{K}')$ refer to site 1 and 2 respectively.

5. EXPERIMENTAL OBSERVATIONS AND EFG PARAMETERS

The experimental proceedure for growing single crystals and cutting in different directions has been described in chapter II. The crystals were ground down to 0.4 mm in order to render them suitable for transmitting the 14.4 keV γ-rays. The experimental results

are tabulated in Table X alongwith the theoretical results calculated from Eq.37 and Eq.38. The results for both the crystals will be discussed separately. The typical spectra for both of these are shown in Fig.26 and Fig.27 separately.

TABLE X

Single crystal absorption peak area ratios for different orientations. Principal values of EFG, assuming Q=+0.40 b for $Fe(NH_4SO_4)_2.6H_2O$ (in units of 10^{17} V/cm^2) V_{xx}= -0.6, V_{yy} = -3.4, V_{zz}= 4.0, for $FeSO_4.7H_2O$, V_{xx} = -3.38, V_{yy}=-4.12 V_{zz} = 7.5.

	Θ	Φ	$Fe(NH_4SO_4)_2.6H_2O$ Expt.(300°K) a_H/a_L	Calc. a_3/a_1	$FeSO_4.7H_2O$ Expt.(300°K) a_H/a_L	Calc.* a_3/a_1
(1)	0	0	0.98	1.00	0.74	0.72
(2)	$\pi/2$	0	1.15	1.15	1.00	0.92
(3)	$\pi/2$	$\pi/4$	2.10	2.16	1.80	1.82
(4)	$\pi/2$	$\pi/2$	0.91	0.88	1.60	1.57
(5)	$\pi/2$	$-\pi/4$	0.54	0.47	0.78	0.78
(6)	$\pi/4$	$\pi/2$	0.90	0.94*	0.83	1.04
(7)	$\pi/4$	0	1.10	1.07*	0.88	0.80
(8)	Powder		0.96	1.00*	0.97	1.00

*Calculated assuming the isotropy of recoilless factor.

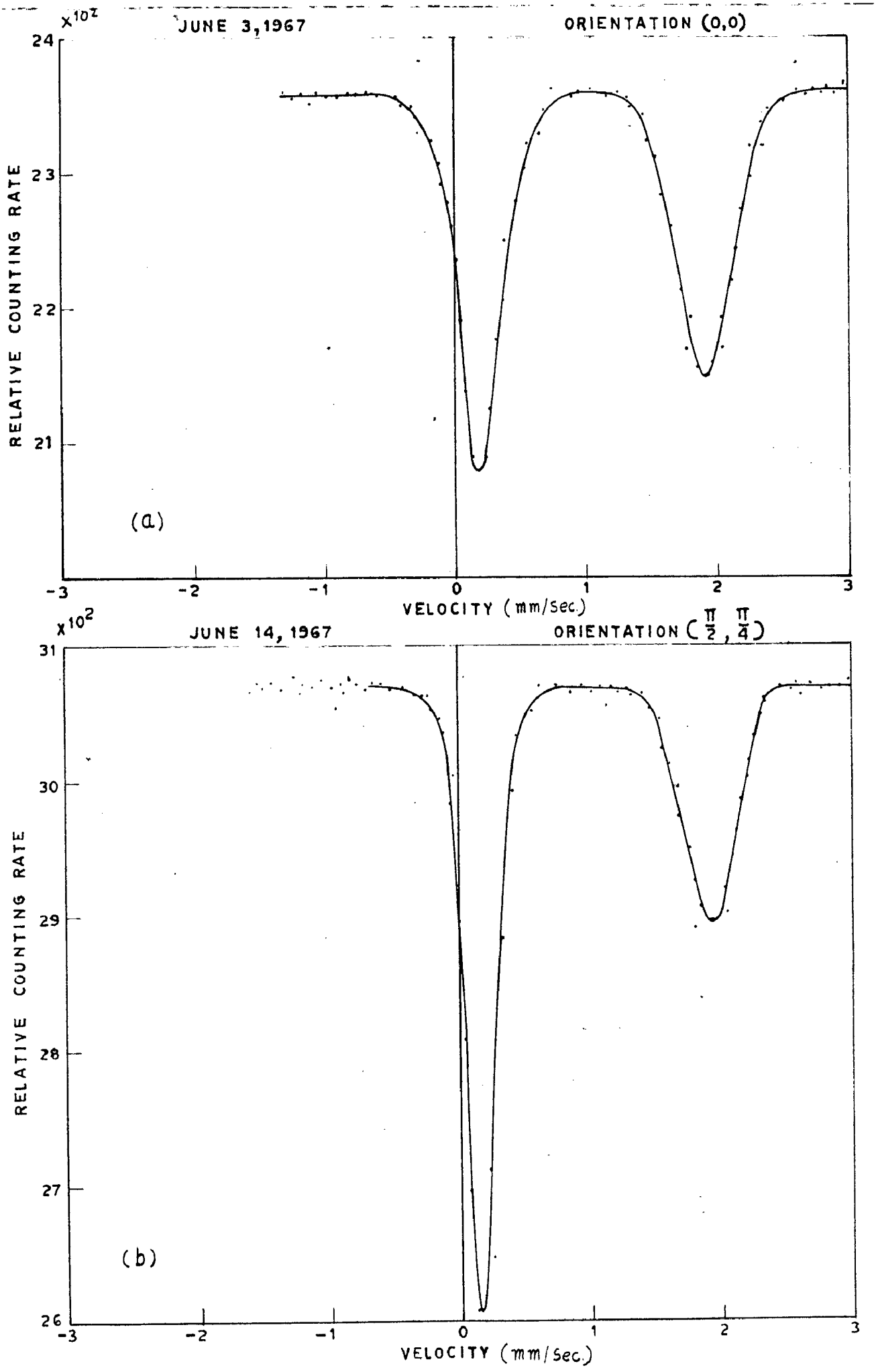

FIG. 26: TYPICAL ABSORPTION SPECTRA FOR SINGLE CRYSTALS OF $Fe(NH_4\ SO_4)_2\ 6H_2O$. THE INCIDENT γ-RAYS SUBTEND ANGLE (a) (0,0) & (b)$(\frac{\pi}{2}, \frac{\pi}{4})$ WITH THE CRYSTAL AXES ($\bar{a}$, $\bar{b}$, $\bar{c}$).

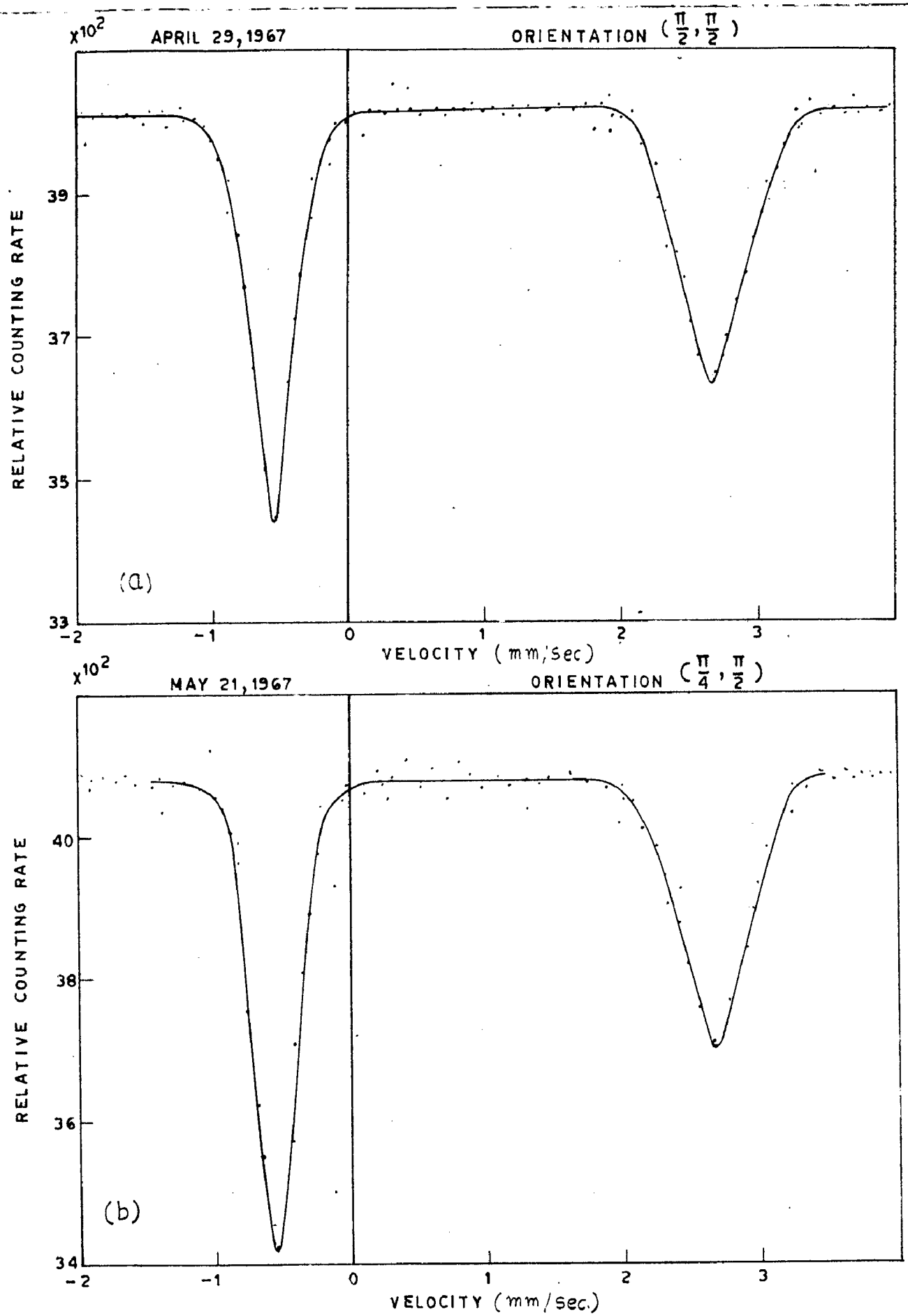

FIG. 27. TYPICAL ABSORPTION SPECTRA FOR SINGLE CRYSTALS OF $FeSO_4 7H_2O$. THE INCIDENT γ-RAYS SUBTEND ANGLE (a) $(\frac{\pi}{2}, \frac{\pi}{2})$ & (b) $(\frac{\pi}{4}, \frac{\pi}{2})$ WITH THE CRYSTAL AXES $(\bar{a}', \bar{b}, c)$

TABLE XI

Direction cosines of EFG axes with respect to the crystallographic axes ($\vec{a}, \vec{b}, \vec{c}$) as calculated from the positional coordinates of H_2O molecules.

Direction cosine	$Fe(NH_4SO_4)_2 \cdot 6H_2O$	$FeSO_4 \cdot 7H_2O$	
		Site 1	Site 2
Za'	0.663	0.759	0.144
Zb	0.472	0.346	0.124
Zc	0.589	0.552	0.981
Ya'	-0.642	-0.677	-0.899
Yb	-0.363	0.121	0.431
Yc	0.693	0.726	0.077
Xa'	-0.610	-0.183	0.414
Xb	0.772	0.924	0.894
Xc	-0.179	-0.328	-0.171

(i) Ferrous Ammonium Sulphate Hexahydrate

The distances and angles* of three sets of water molecules surrounding the Fe^{++} are given in Fig.28. The angles between the different axes of octahedron are nearly 90° and these directions are taken as the axes of the EFG. The experimental observations on area ratios could be reconciled with the theoretical predictions based on Eq.37, Table X, only when the following specifications of EFG parameters are made:

(a) The OW(9)-OW(9) direction is the major axis i.e. $\hat{Z}$-axis of EFG, whereas the OW(7)-OW(7) and OW(8)-OW(8) directions correspond to the $\hat{Y}$ and $\hat{X}$ axes respectively. The direction cosines of $(\hat{X},\hat{Y},\hat{Z})$ axes relative to $(\vec{a},\vec{b},\vec{c})$ axes calculated from Fig.22 and Table VIII are tabulated in Table XI.

(b) The ratio of the higher energy experimental peak occurring at $\simeq 1.95$ mm/sec to the lower energy one at $\simeq 0.15$ mm/sec is a_3/a_1 and not a_1/a_3. This implies that $\pm 3/2 \longrightarrow \pm 1/2$ transition is higher in energy relative to $\pm 1/2 \longrightarrow \pm 1/2$ transition and from Eq.31, assuming Q to be equal to $0.40b$[21], we find that $eq = +4.0\times10^{17} V/cm^2$ ($300^{\circ}K$).

(c) $\eta = 0.7$

---

*As no x-ray data is available for $Fe(NH_4SO_4)_2.6H_2O$, the distances and angles referred to here are those for its isomorphous salt $Zn(NH_4SO_4)_2.6H_2O$[16].

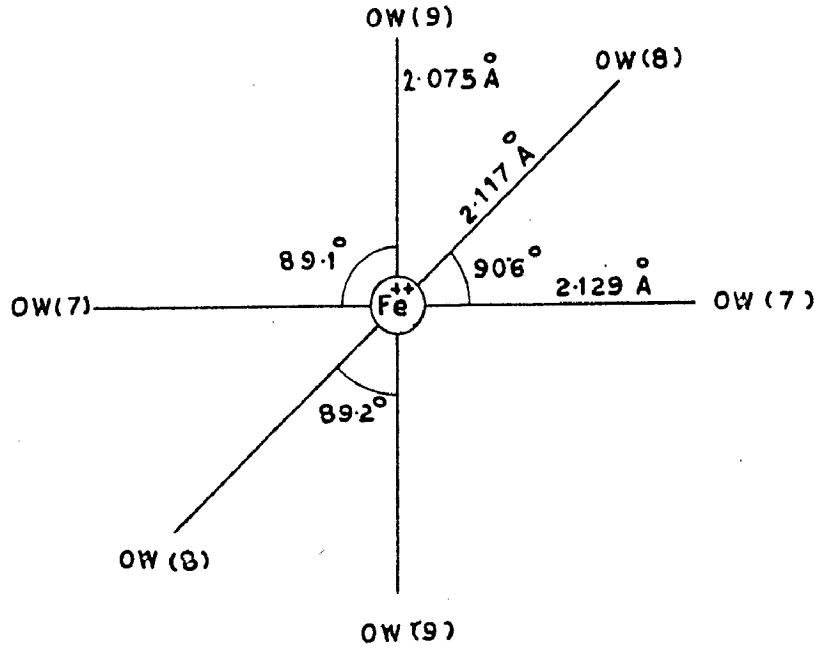

FIG.28. SCHEMATICS OF $Zn(NH_4SO_4)_2.6H_2O$ (ISOMORPHOUS WITH $Fe(NH_4SO_4)_2.6H_2O$ CRYSTAL SHOWING DISTANCES BETWEEN THE WATER MOLECULES AROUND Fe^{++} AND ANGLES BETWEEN OCTAHEDRON AXES.

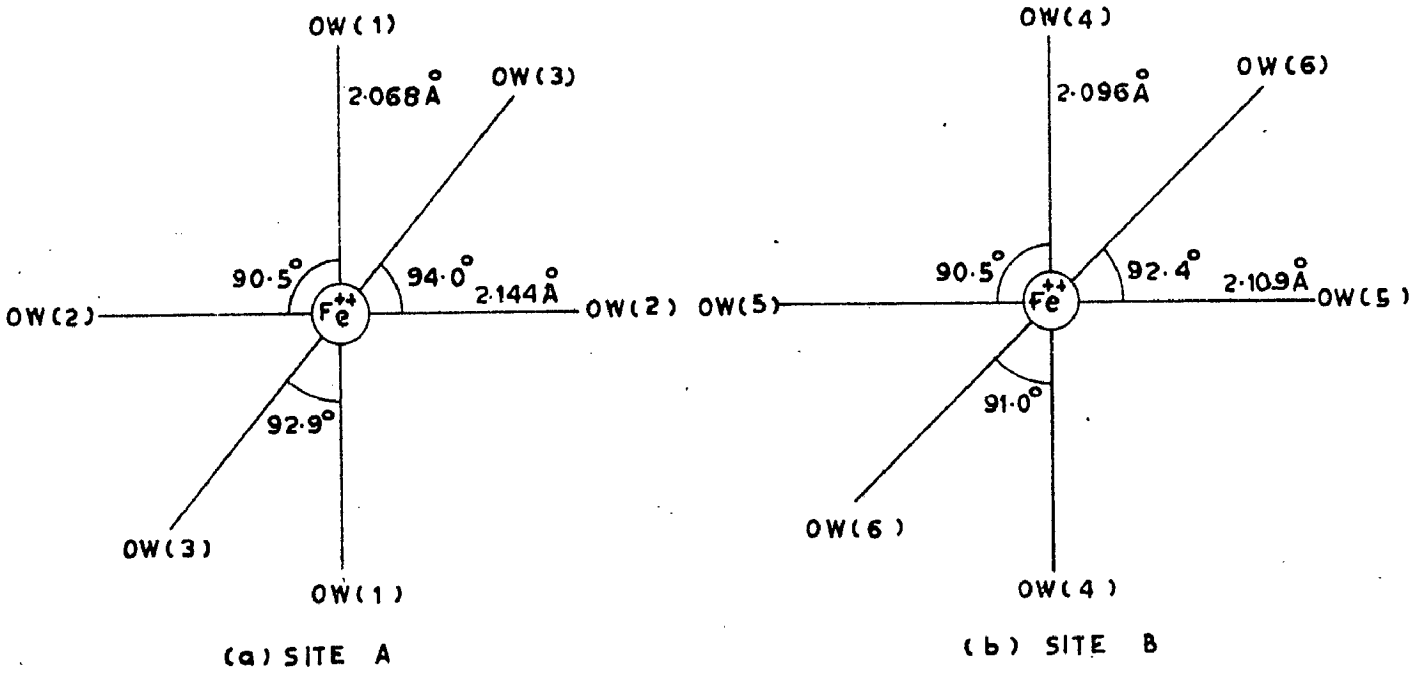

FIG. 29. THE SCHEMATIC ARRANGEMENT FOR $FeSO_4.7H_2O$ CRYSTAL SHOWING DISTANCES BETWEEN H_2O MOLECULES AROUND Fe^{++} AND ANGLES BETWEEN THE OCTAHEDRON AXES FOR SITE A AND SITE B.

For the measurements in the orientations (1) through (5), it can be shown that $P_3(\theta_1, \phi_1) = P_3(\theta_2, \phi_2)$ and $P_1(\theta_1, \phi_1) = P_1(\theta_2, \phi_2)$ and f' cancels out of Eq.37, so that the calculated values are valid even in the presence of anisotropy. But the comparision of the values for orientations (6) and (7) indicates that f' anisotropy is not important at the room temperature. The assignment is quite unique since the same set of five parameters of EFG tensor is able to satisfy the observations at all of the (1) to (7), settings.

(ii) Ferrous Sulphate Heptahydrate

There are 4 molecules per unit cell and these form two distinct sites 1 and 2 (each site includes the site having the point symmetry $\bar{1}$). The schematics of the arrangement of six water molecules around Fe^{++} are given in Fig.29(a) and Fig.29(b) for each set separately.

Likewise in this case the angles between the different axes of the octahedron are nearly 90° and these directions are taken as the axes of the EFG. The direction cosines of the axes $(\hat{X}, \hat{Y}, \hat{Z})$ relative to $(\vec{a}, \vec{b}, \vec{c})$ as determined from the positional coordinates of the water molecules are tabulated in Table XI. The experimental results of the absorption peak areas are measured for different orientations and are tabulated in Table X alongwith the values calculated from Eq.38. The calculations are based on the following assumptions regarding the

EFG axes and asymmetry parameters.

(a) For site 1 OW(1)-OW(1) direction is the $\hat{Z}$ axis; OW(2)-OW(2), the $\hat{Y}$-axis and OW(3)-OW(3), the $\hat{X}$-axis. For site 2, OW(4)-OW(4) is taken as the $\hat{Z}$ axis of EFG, OW(5)-OW(5), the $\hat{X}$-axis and OW(6)-OW(6), the $\hat{Y}$-axis.

(b) The ratio of the higher energy experimental peak occurring at $\simeq$ + 2.55 mm/sec to the lower-energy one at $\simeq$ -0.56 mm/sec is $\frac{a_3}{a_1}$ and not $\frac{a_1}{a_3}$, implying thereby that sign of q is positive. The value of eq = $+7.5 \times 10^{17}$ V/cm^2 (300°K).

(c) $\eta = 0.1$ for sites 1 and 2

It may be remarked that f does not cancel out of Eq.38 for any orientation, (1) to (7), since for the two special sites 1 and 2, the relative absorption probabilities are different $\left[p_{3_1}(\theta_1, \phi_1) \neq p_{3_1}(\theta_2, \phi_2) \right]$. From the agreement between the experimental values and those calculated assuming the isotropy of f′, one concludes that for $FeSO_4.7H_2O$ the anisotropy in the Lamb-Mössbauer fraction is inappreciable at room temperature within the experimental errors. The assignment of the parameters of EFG is quite unique since the requirement was more stringent due to the presence of two sites 1 and 2 per unit cell.

6. DISCUSSION

The sign of the nuclear quadrupole coupling constant

R E S U M E

The Mössbauer effect, viz. resonance absorption of recoillessly emitted gamma rays, has been used as a tool for the study of hyperfine interactions in iron compounds, where the Fe^{2+} or Fe^{3+} ion is in a ligand field of octahedral symmetry. Chapter I is introductory in content and discusses the different hyperfine interactions in a sketchy manner. Moreover all the compounds studied belong to the octahedral point group O_h of the ligands, the splitting of the orbital degeneracy in the presence of octahedral ligand field is discussed.

The Mössbauer spectrometer was fabricated locally and employed a constant velocity cam mechanical drive for Doppler tunning the source. The relevant details of its fabrication and salient features of its operation constitute the subject matter of chapter II.

Chapter III deals with a systematic study of the ferro and ferricyanide super complexes with 3d-transition elements viz. Cr, Mn, Fe, Co, Ni, Cu and Zn. On the basis of observed values of isomer shifts, it is concluded that the coordination number of Fe^{2+} remains six and it is bounded covalently with the carbon atom of the (CN^{-}) group. Furthermore a metal-metal charge transfer is invoked to explain the change of I.S. The nearly double values of quadrupole splittings in ferricyanide super complexes (except for Mn^{2+} and Zn^{2+}) as compared to

and on that basis the conclusion that the ground state orbital wave function is a singlet $|xy\rangle$ both in the case of $Fe(NH_4SO_4)_2.6H_2O$ and $FeSO_4.7H_2O$ agrees with that given by Ingalls[82] and Grant et al[75]. By means of the magnetic perturbation technique, Grant et al had set the lower limit of $\eta > 0.7$ for $Fe(NH_4SO_4)_2.6H_2O$, which agrees with our value of η . The large value of asymmetry parameter arises due to the asymmetric distribution of $(NH_4)^+$ ions around Fe^{++}. Furthermore the anisotropy in the Lamb-Mössbauer fraction for $FeSO_4.7H_2O$ is inappreciable at room temperature within the experimental errors.

Measurements of magnetic anisotropy and susceptibility of single crystals had been reported and accounted for in the case of ferrous ammonium sulphate by a number of workers[86-88]. Thakurta and Mukhopadhyay[86] infer that the magnetic ellipsoid of the crystals are roughly reduced to oblate spheroids about the χ_2 axis, which has the maximum susceptibility. Furthermore the "b" axis coincides with the principal susceptibility and the angle between "$\vec{a}$" and χ_1 axes is $\simeq -37^0$. The principal axes of EFG tensor as determined in our measurements do not coincide with the principal axes of susceptibility tensor. Such was also the case with $FeCl_2.4H_2O$[74]. No report of the measurements of magnetic anisotropy of $FeSO_4.7H_2O$ exists in literature.

$K_3Fe^{III}(CN)_6$ are explained on the basis of ground state wave functions.

Nuclear Electric Field Gradient Tensor parameters for the single crystals of $Fe(NH_4SO_4)_2.6H_2O$ and $FeSO_4;7H_2O$ have been determined and described in chapter IV. The method utilizes the fact that for single crystals the area ratios of the quadrupole doublet vary as a function of the angle which the EFG principal axes make with the incident γ-ray direction. The experimental values are compared with the calculated ones, the latter being based on the assumption that the recoilless fraction f' is isotropic. It is concluded that in $FeSO_4.7H_2O$, f' is isotropic at 300°K within the accuracy of the method.

REFERENCES

1. A.C.G. Mitchell and M.W. Zemansky, "Resonance Radiation and Excited Atoms," (Cambridge University Press, 1934, Reprinted 1963).

2. P.P. Moon, Proc. Phys. Soc.(London) 64, 76 (1951).

3. R.L. Mössbauer, Z. Physik, 151, 124 (1958).

4. K.G. Malmfors, Resonant Scattering of Gamma Rays. In "Beta and Gamma Ray Spectroscopy", K. Siegbahn, ed., Chap. 18 (North Holland, Amsterdam, 1955).

5. F.R. Metzger, Progr. Nucl. Phys. 7, 53 (1959).

6. W.E. Lamb, Phys. Rev. 55, 190 (1939).

7. H. Fraunfelder, "The Mössbauer Effect" (W.A. Benjamin, Inc., New York, 1962).

8. K.G. Malinfors, R.L. Mössbauer, "Nuclear Resonance Fluorescence of Gamma Radiation", Alpha, Beta, Gamma Spectroscopy, K. Siegbahn, ed. (North Holland Publishing Co., Amsterdam, 1965) p.1281.

9. R.L. Mössbauer, Ann. Rev. Nucl. Sci. 12, 123 (1962).

10. A.J.F. Boyle and H.E. Hall, Reports on Prog. in Phys. 25, 441 (1962).

11. G.K. Wertheim, "Mössbauer Effect, Principle and Applications", (Academic Press, New York, 1964).

12. H. Fraunfelder, H. Lustig, eds., "Mössbauer Effect, Recoilless Emission and Absorption of Gamma Rays, Proc. of the First International Conference on the Mössbauer Effect, University of Illinois (1960), U.S. Air Force Report.

13. D.J.M. Compton, A.J. Shoen, eds., Proc. of the Second International Conference on the Mössbauer Effect (Sacley, France, 1961, Wiley, New York, 1962).

14. V.P. Alfimenkov and A.V. Strelkov, eds., Proc. of the Conference on the Mössbauer Effect, Dubna, USSR, 1962 (Joint Institute for Nuclear Research Dubna, 1963) (In Russian)/Translation (Consultant Bureau Enterprises, Inc., New York, 1963).

15. A.J. Bearden, ed., Proc. of the Third International Conference on the Mössbauer Effect, Rev. Mod. Phys. 36, 333 (1964).

16. I.J. Gruverman, ed., "Mössbauer Methodology", (Plenum Press, New York, 1965).

17. International Atomic Energy Agency, Proc. of a Meeting of the Advisory Pannel on Mössbauer Spectroscopy, Vienna, Austria, April, 1965.

18. V. Weisskopf, The Mössbauer Effect, in W.E. Brittin and B.W. Downs (eds.), "Lectures in Theoretical Physics", (InterScience, New York, 1961) Vol.3, p.70.

19. H.J. Lipkin, Ann. Phys. 9, 332 (1960); 18, 182 (1962).

20. E. Cotton, J. Phys. Radium 21, 265 (1960).

21. J.O. Artman, Phys. Rev. 143, 541 (1966).

22. R.D. Evans, "The Atomic Nucleus", (Mc Graw Hill, New York, 1955) p. 165.

23. A.R. Bodmer, Nucl. Phys. 21, 347 (1960).

24. O.C. Kistner and A.W. Sunyar, Phys. Rev. Lett. 8, 436 (1962).

25. A.C. Melissinos and S.P. Davis, Phys. Rev. 115, 130 (1959); and W.J. Tomlinson, III and H.H. Stroke, Phys. Rev. Lett. 8, 436 (1962).

26. D.A. Shirley, Rev. Mod. Phys. 36, 339 (1964).

27. R.E. Watson and A.J. Freeman, Phys. Rev. 120, 1125(1960).

28. E. Fermi and E. Segre, Z. Physik 82, 729 (1933); S.A. Goudsmit, Phys. Rev. 43, 636 (1933).

29. G.K. Wertheim and R.H. Herber, J. Chem. Phys.36, 2497 (1962).

30. A.J. F. Duncan and R.M. Golding, Quat. Rev. (London) 19, 36 (1965).

31. W.J. Nicholson, G. Burns, Phys. Rev. 129, 2490 (1963).

32. V.I. Goldanskii, E.F. Makarov and V.V. Khrapov, Soviet Phys. JETP 17, 508 (1963); Phys. Lett. 3, 344 (1963).

33. R.B. King, R.H. Herber and G.K. Wertheim, Inorg.Chem. 3, 101 (1964).

34. L.W. Fagg and S.S. Hanna, Rev. Mod. Phys. 31, 711 (1959)

35. E.M. Condon and G.H. Shortley, "Theory of Atomic Spectra," (Cambridge University Press; 1935).

36. R.S. Preston, S.S. Hanna, and J. Heberle, Phys. Rev. 128, 2207 (1962).

37. R.V. Pound and G.A. Rebka, Jr., Phys. Rev. Lett. 3, 554 (1959).

38. C.J. Ballahausen, "Introduction to Ligand Field Theory" (Mc Graw-Hill Book Company, Inc., New York, 1964).

39. L. Loevborg, Nucl. Instr. Methods, 34, 307 (1965).

40. M. Boronaz, G. Filoti, A. Gelberg, U. Granbari and C. Nistor; Nucl. Instr. Methods, 40, 60 (1966).

41. D.S.P. Bunbury, J. Sci. Instr., 43,783 (1966).

42. R.L. Cohn, Rev. Sci. Instr. 37, 957 (1967).

43. H. Brafman, M. Greenshpan and R.H. Herber, Nucl. Instr. Method, 42, 245 (1966).

44. K.C. Tripathi, Ark. Fys (Sweden) Vol. 30, paper 570 (1965) (Swedinsch, Physics Conference Uppsala 1965).

45. C.W. Kocher, Rev. Sci. Instr., 36, 1018 (1965).

46. A.D. Adler and M. Hane, Am. J. Phys. 34, 189 (1966).

47. P.M. Valov, U.K. Sokolova, A.G. Vilenskii and E.E. Vainshtein Instrum. Exper. Tech. (U.S.A.) 5, 1186 (1966).

48. R.M. Housley, N.E. Erickson and J.G. Dash, Nucl. Instr. Methods, 27, 29 (1964).

49. H. Lustig, Am. J. Phys. 29, 1 (1961).

50. S. Margulies and J.R. Ehrman, Nucl. Instr. Methods 12, 131, (1961).

51. R.L. Collins and R. Pettit, J. Am. Chem. Soc. 85, 2332 (1963).

52. M.B. Robin, Inorg. Chem. 1, 337 (1962).

53. A.F. Wells "Structural Inorganic Chemistry" 3rd ed. (Oxford, at the Clearence Press, 1962) p.740.

54. J.F. Keggin and F.D. Miles, Nature 137, 577 (1936).

55. W.E. Prout, E.R. Russell, and H.J. Groh, J. Inorg. Nucl. Chem. 27, 473 (1965).

56. E.S. Dana, " A Text Book of Mineralogy" (John Wiley and Sons. Inc., New York, 1932).

57. C. Palache, (the late) H. Barman and C. Frondel "Dana's System of Mineralogy" (John Wiley and Sons Inc. New York, 1951) Vol.II, p. 499.

58. J. Danon, J. Chem. Phys. 41, 3378 (1964).

59. W. Kerler, Z. Physik 175, 200 (1963).

60. J. Matas and T. Zemcik, Phys. Lett. 19, 111 (1965).

61. J.F. Duncan and P.W.R. Wigley, J. Chem. Soc. 1120(1963).

62. L. Pauling, "The Nature of Chemical Bond"(Cornell University Press, Ithaca, New York, 1960).

63. Thorpe's Dictionary of Applied Chemistry (Longmans Green and Co. Ltd. London, 1961), Vol.3, P.478.

64. A.E. Douglas and P.M. Routly, Astrophys. J.(Suppl.) 295 (1955); P.K. Carroll, Can. J. Phys. 34, 85 (1956).

65. T.P. Das and E.L. Hahn, Solid State Physics, F. Seitz and D. Turnbull eds. (Academic Press Inc., New York, 1958) Supl.1.

66. R. Bersohn, J. Chem. Phys. 20, 1505 (1952).

67. C. Alff and G.K. Wertheim, Phys. Rev.122, 1414 (1961).

68. G.K. Wertheim, Phys. Rev. 121, 63 (1961).

69. C.E. Johnson, Proc. Phys. Soc. 88, 943 (1966).

70. K. Ono and A Ito, J. Phys. Soc. Japan 19, 899 (1964).

71. C.E. Johnson, W. Marshall, and G.J. Perlow, Phys. Rev. 126, 1503 (1962).

72. U. Gonser and R.W. Grant, Biophys. J. 5, 823 (1965).

73. S.L. Ruby and P.A. Flinn, Rev. Mod. Phys. 36,351(1964).

74. R.L. Collins, J. Chem. Phys. 42, 1072 (1965).

75. R.W. Grant, H. Wiedersich, A.H. Muir, Jr, U.Gonser, and W.N. Delgass, J.Chem.Phys.45, 1015 (1966).

76. P. Zory, Phys. Rev. 140, A1401 (1965).

77. M. Kalvius, U. Zahn, P. Kienle and H. Eicher, Z. Naturforsch 172, 494 (1962).

78. P. Kiele, Physik Verhandl 2/3, 33 (1963).

79. W. Hofmann, Z. Krist. 78, 278 (1931); H. Montgomery and E.C. Lingafelter, Acta Cryst. 17, 1479 (1964).

80. W.H. Baur, Acta Cryst. 17, 1167 (1964).

81. B. Bleaney and K.W.H. Stevens, Reports Prog.Phys. 16, 108, (1953).

82. R. Ingalls, Phys. Rev. 133, A787 (1964).

83. G. Lang, Nucl. Instr. Methods 24, 425 (1963).

84. G.T. Ewan, R.L. Graham, and J.S. Geiger, Nucl. Phys. 19, 221 (1960).

85. M.E. Rose, "Elementry Theory of Angular Momentum", (John Wiley and Sons, Inc., New York, 1957).

86. A. Bose, A.S. Chakravarty and R. Chaterjee, Proc. Roy. Soc. (London) A261, 207(1961).

87. B.D. Bhattacharya, Ind. J. Phys. 38, 311 (1964).

88. D.G. Thakurta and D. Mukhopadhyay, Ind. J. Phys. 40, 69 (1966).

LIST OF PUBLICATIONS

(a) (included in the thesis)

1. K. Chandra, Deo Raj and S.P. Puri, Mössbauer Studies of Ferro-and Ferricynide Super Complexes with 3d Transition Elements
   J. Chem. Phys. Vol.46, No.4,pp.1466-1468, 1967.

2. K. Chandra and S.P. Puri, Nuclear Electric Field Gradient Determination in $Fe(NH_4SO_4)_2.6H_2O$ and $FeSO_4.7H_2O$ single crystals
   Phys. Rev. (communicated).

(b) (not included in the thesis)

3. Deo Raj, K. Chandra and S.P. Puri, Mössbauer Studies of Chalcopyrite
   J. Phys. Soc. Japan (In press).

4. Deo Raj, K. Chandra and S.P. Puri, Crystal Field Splitting in Iron Tutton Salts by Mössbauer Effect
   J. Phys. Soc. Japan (In press).